学位論文

# Functional analysis of Ripply2, a suppressor of Tbx6, in mouse somitogenesis

（マウスの体節形成における **Tbx6** 抑制因子 **Ripply2** の機能解析）

平成 **25** 年 **12** 月　博士（理学）申請

東京大学大学院理学系研究科

生物科学専攻

趙　薇

## Abstract

Somites are transient reiterated structure formed in paraxial mesoderm, in which a block of the anterior end of the presomitic mesoderm (PSM) buds off in every 2 hours in mouse. During mouse somitogenesis, anterior limit of Tbx6 protein is thought to be important for accurate somite segmentation. This anterior limit is defined by Mesp2, which transcription is induced by Tbx6 and in turn promotes the degradation of Tbx6 at the segmentation boundary of newly forming somite. *Ripply2*, a Mesp2 target, is proposed to be involved in this down-regulation because *Ripply2* deficiency causes an anterior expansion of the Tbx6 domain, resembling the *Mesp2*-null phenotype. However, it is unclear whether Ripply2 acts on Tbx6 independently or in association with Mesp2. To address this question, I generated three sets of transgenic mice with following Ripply2 expression patterns: 1) overexpression at the endogenous expression domain, 2) expression instead of *Mesp2* (*Ripply2*-knockin), and 3) ectopic expression in the entire PSM. I found accelerated Tbx6 degradation in the embryos showing Ripply2 overexpression accompanied by the down-regulation of Mesp2. In the *Ripply2*-knockin embryos, the anterior limit of Tbx6 domain was generated by Ripply2 even in the absence of Mesp2. These observations clearly demonstrate that Tbx6 degradation is Ripply2-mediated, without Mesp2 involvement. Ectopic Ripply2 expression along the entire PSM suppressed Tbx6 and induced Sox2-positive neural tube formation at the bilateral domain, resembling the *Tbx6*-null phenotype. This phenotype was resulted from elimination of Tbx6 protein but not mRNA, suggesting the post-translational down-regulation of Tbx6 by Ripply2. Taken together, my results demonstrate that Ripply2 represses Tbx6 in a Mesp2-independent manner, which contributes to the accurate segmental border formation. Further, the direct interaction between Ripply2 and Tbx6 was fully proved by a series of biochemical analyses including GST pull-down assays. These results support that Ripply2 is essential for somitogenesis by repressing Tbx6.

## Contents

# Introduction

Somites are reiterant structures in vertebrate embryos derived from the paraxial mesoderm flanking the notochord and neural tube, and subsequently give rise to vertebra, axial muscle, early blood vessels, and peripheral spinal nervous (Borycki and Emerson, 2000; Brand-Saberi and Christ, 2000; Monsoro-Burq and Le Douarin, 2000). Somites are epithelial blocks of mesoderm and form rhythmically from the presomitic mesoderm (PSM) at a time period that is characteristic of the species, ranging from 30 minutes in zebrafish embryos, 90 minutes in chicken and 120 minutes in mouse, to approximately 4-5 hours in humans. The somitogenesis begins from the anterior part immediately caudal to the otic vesicle and runs posteriorly on both sides of the neural tube and notochord to the caudal tip of the embryo (Fig. 1). Pairs of somites regularly segment synchronously from the anterior region of the presomitic mesoderm (PSM) in an anterior-to-posterior sequence until a defined number is reached (Couly et al., 1993). The strict temporal and spatial regulation of somitogenesis is crucial. For the past decade, theoretical model called “clock and wavefront model” is proposed (Fig. 2). An oscillatory clock, composed of kinds of cycling genes, which expresses on and off in the PSM, establishes temporal periodicity in somitogenesis. It has recently been found that the Notch signaling pathway makes synchronized oscillation among neighboring PSM cells through the Delta-Notch loop, resulting in a smooth transcriptional wave that sweeps through the PSM. The basic helix-loop-helix (bHLH) factor Hes7, an effector of Notch signaling, plays a central role in generating a two-hour oscillatory cycle of Notch signaling *via* a negative feedback loop (Bessho et al., 2003). The cycle operates within somite precursor cells and stops when they reach a specific stage of maturation defined as a “wavefront”, which is established in a manner dependent on the antagonistic interaction between FGF and retinoic acid (RA)-signaling gradients (Delfini et al., 2005; Diez del Corral et al., 2003; Dubrulle et al., 2001; Moreno and Kintner, 2004; Sawada et al., 2001; Wahl et al., 2007). This arrest translates the temporal oscillations into a timed spatial event, namely, boundary formation.

Tbx6, a T-box transcriptional factor, is expressed in the PSM and has a clear anterior limit demarcadting a potential segmental border. During a somite cycle, Notch signaling and Tbx6 together induce the expression of a bHLH transcription factor mesoderm posterior protein 2 (Mesp2) (Yasuhiko et al., 2006), which induces the expression of the genes involved in rostro-caudal polarity and PSM cells epithelialization. The anterior boundary of Mesp2 expression domain determines the position of new somite segmentation. *Mesp2*-null embryos fail to segment and that the resulting non-segmented mesoderm shows caudalized property (Fig 3. B) (Saga et al., 1997). The anterior limits of *Mesp2* and *Tbx6* expression domains overlap accurately, and Tbx6 protein disappears from this region after Mesp2 expression. Therefore, in each cycle, the Tbx6 domain recedes posteriorly by one somite length and thus, defines the next Mesp2 expression domain. In this regulation, Mesp2 suppresses its own upstream regulator Tbx6. Interestingly, the *Tbx6* mRNA domain remains unchanged even in the *Mesp2*-null embryos, indicating that Mesp2 suppresses Tbx6 at the post-transcriptional level (Oginuma et al., 2008b). Further, the Mesp2 target Ripply2 is also involved in this negative regulation. Ripply2 turned out to be a negative regulator of Mesp2, and is essential for periodic generation of the rostro-caudal polarity within a somite. In contrast to *Mesp2*-null mice, *Ripply2*-null embryos show a rostralized phenotype, with prolonged expression of Mesp2 (Morimoto et al., 2007). *Ripply1/2*-deficient embryos exhibited enhanced Tbx6 anterior expansion and Mesp2 up-regulation (Fig 3. C) (Takahashi et al., 2010), suggesting that Ripply1/2 regulates Mesp2 expression by modulating elimination of Tbx6 proteins. As putative transcriptional repressors genes, *Ripply* family members in other vertebrate species include genes required for precise formation of the somite boundary during somitogenesis (Chan et al., 2007; Chan et al., 2006; Kawamura et al., 2005; Kondow et al., 2006). Zebrafish *ripply1*, a homolog of mouse *Ripply2*, can convert tbx6 (previously called tbx24) from a transcriptional activator to a repressor (Kawamura et al., 2008). *Xenopus* Bowline (Ripply2) represses Tbx6 *via* association with the transcriptional co-repressor

XGrg-4 (Groucho/TLE) (Hitachi et al., 2009; Kondow et al., 2007).

However, so far, the molecular mechanism of the Ripply2-mediated degradation is largely unknown. In this study, I make efforts to clarify the question whether Ripply2 directly degrades Tbx6 protein independent of Mesp2. Using Ripply2-overexpressing transgenic (TG) mice, I found that Ripply2 is more important in Tbx6 degradation than Mesp2, as Tbx6 degradation was accelerated under the condition of up-regulated Ripply2 and down-regulated Mesp2. Mesp2-independent degradation was further verified using mice that *Mesp2* was replaced with *Ripply2*, in which Ripply2 successfully retained Tbx6 anterior limit. I also induced ectopic Ripply2 expression in the posterior PSM. These embryos showed a *Tbx6*-null-like phenotype, which led us to conclude that Ripply2 can suppress Tbx6 protein in the entire PSM. Finally, I proved that Ripply2 directly participates in this degradation *via* showing its interaction with Tbx6 protein.

# Result

***Ripply2* overexpression caused caudalization of somite by down-regulation of Mesp2**

I speculate with previous observations that either Mesp2 (Oginuma et al., 2008b) or Ripply2 (Takahashi et al., 2010) can lead to degradation of Tbx6. However, loss of *Ripply2* results in the prolonged expression of *Mesp2* but stabilizes Tbx6. This finding suggests that Mesp2 alone cannot induce Tbx6 degradation, indicating the possibility that Tbx6 suppression is a Mesp2-independent and Ripply2-dependent process (Hypothesis-1). Considering that both *Mesp2*-null and *Ripply2*-null embryos show Tbx6 domain expansion, both factors might be essential but not sufficient for Tbx6 destabilization (Hypothesis-2) (Fig. 4). To investigate these two hypotheses, I generated Ripply2 overexpression mouse transgenic (TG) with endogenous Ripply2 expression pattern (Fig. 5A).

The *FLAG-Ripply2* TG mice showed defective vertebral formation such as shortened trunk and short and kinked tail (Fig. 5B). First, I examined whether the FLAG-Ripply2 retained functions of the endogenous protein through a rescue experiment. To this end, the transgene was introduced into *Ripply2*-null background. *Ripply2*-null embryos displayed no clear segmental borders and died soon after birth with a short trunk and tail, similar to findings reported previously (Morimoto et al., 2007). The *FLAG-Ripply2*;*Ripply2*-null mice survived into the adult stage, indicating that FLAG-Ripply2 could functionally replace the endogenous Ripply2. However, the *FLAG-Ripply2*;*Ripply2*-null mice still showed kinked and shortened tail, similar to that observed in the *FLAG-Ripply2* mice (Fig. 5C). I speculated this could be due to the high dose of Flag-Ripply2 expressed even in the *Ripply2*-null background (Fig. 6A and 7E-F).

Next, I prepared embryonic skeletal samples from E18.5 embryos to investigate the influence of FLAG-Rippy2 overexpression. In contrast to *Ripply2*-null fetuses, which showed a rostralized phenotype with fewer pedicles of neural arches (Fig. 8C), the phenotype of *FLAG-Ripply2* TG fetuses resembled that of *Mesp2*-null fetuses, which show a caudalized somitic mesoderm with extensive fusion of the pedicles in the neural arches (Fig. 8B) (Saga et al., 1997).

The *FLAG-Ripply2*;*Ripply2*-null embryos showed more caudalized phenotype compared with WT fetus (Fig. 8A), but not to the extent seen in *FLAG-Ripply2* mice (Fig. 8E). Furthermore, *FLAG-Ripply2*;*Ripply2*$^{+/-}$ mice exhibited a moderate degree of pedicle fusion, between that of *FLAG-Ripply2*;*Ripply2*-null and *FLAG-Ripply2* embryos (Fig. 8D). These results indicate that Ripply2-overexpression led to the caudalization of the somites.

***Ripply2* overexpression caused caudalization of somite by down-regulation of Mesp2**

The rostro-caudal patterning was further examined by marker genes expression analyses by using whole-mount *in situ* hybridization. In WT embryos, the expression of the caudal marker *Uncx4.1* and *Dll1* were restricted to the caudal compartments of the somites (Fig. 8F and 9C); the expression of *Tbx18* was restricted to the rostral half of the segmented somites (Fig. 8K) (Bussen et al., 2004; Kraus et al., 2001). Although the *FLAG-Ripply2* TG embryos exhibited almost unchanged expression of *Uncx4.1* and *Dll1* compared with WT (Fig. 8G and 9D), their expression of *Tbx18* was down-regulated (Fig. 8L) indicating that the degree of caudalization is much weaker than that in *Mesp2*-null embryos (Takahashi et al., 2000). The phenotype of *FLAG-Ripply2* TG was contrary to that of *Ripply2-null* embryos, in which *Uncx4.1* was greatly reduced (Fig. 8H), whereas *Tbx18* domain expanded to cover the entire somite region (Fig. 8M). *In the FLAG-Ripply2;Ripply2*-null embryos, the rostralized expression pattern was compensated to give a phenotype comparable to that of the WT (Fig. 8O). The caudalization in *FLAG-Ripply2* embryos was weakened by crossing them with *Ripply2-null* mice (Fig. 8J), judged by *Uncx4.1* and *Tbx18* expression in *FLAG-Ripply2;Ripply2*$^{+/-}$ (Fig. 8I, N). The expression dosages of rostral and caudal markers were proportional to that of *Ripply2* mRNA, indicating that Ripply2 dosage influences rostral-caudal patterning of the somites.

The underlying cause of the polarity alteration in somites was determined by the study of

gene expression profiles of *Tbx6*, *Ripply2*, and *Mesp2*. There was no apparent change observed in *Tbx6* expression in *FLAG-Ripply2* embryos (Fig. 9A, B). *Ripply2* expression showed two patterns in the WT embryos; a single stripe at S-1 of the anterior PSM, as well as two obscure stripes at S0 and S-1 (Fig. 10A). In *FLAG-Ripply2* embryos, there were several broad stripes of *Ripply2* in the PSM and somitic region, and sometimes the expression was also observed in the neural tube (Fig. 10D). *Ripply2* expression was restored in *FLAG-Ripply2*;*Ripply2*$^{+/-}$ (Fig. 10E) and *FLAG-Ripply2*;*Ripply2*-null (Fig. 10F) embryos compared with *Ripply2*-null embryos (Fig. 10C). During somitogenesis, WT embryos generally showed a single *Mesp2* stripe of variable width and faint expression depends on the segmentation cycle (Fig. 10G). *Mesp2* expression domain was broader in *Ripply2*-null embryos compared to WT embryos and two of the three *Ripply2*-null embryos showed two clear *Mesp2* stripes rather than the usual single *Mesp2* strip in WT embryos (Fig. 10I). Further, *Ripply2*$^{+/-}$ embryos also showed expanded *Mesp2* expression, indicating that *Ripply2* dosage influences the regulation of its up-stream factor, *Mesp2* (Fig. 10H). In addition, the *Mesp2* mRNA in *FLAG-Ripply2* TG embryos was down-regulated (Fig. 10J). *Mesp2* expression in the *FLAG-Ripply2*;*Ripply2*$^{+/-}$ and *FLAG-Ripply2*;*Ripply2*-null embryos decreased compared to that in the *Ripply2*-null embryo (Fig. 10K, L). This observation is in agreement with the previous finding that Ripply2 is a negative regulator of *Mesp2*, and is involved in rostro-caudal patterning via affecting *Mesp2* expression (Morimoto et al., 2007). Based on these findings, the cause of partially caudalized phenotype observed in *FLAG-Ripply2* mice could be ascribed to the reduction of *Mesp2* expression.

### ***Ripply2*** **overexpression accelerated Tbx6 degradation**

To examine the expression of Ripply2 protein, which has never been examined previously, I generated an anti-Ripply2 antibody. The specificity of this antibody was confirmed by western

blotting (Fig. 11A). I used the Ripply2 antibody to stain WT and *Ripply2*-null embryos and observed the Ripply2 signal only in the WT but not in *Ripply2*-null embryos (Fig. 11B, C). This further confirms the specificity of the Ripply2 antibody. In *FLAG-Ripply2* embryos, Ripply2 could be detected by immunostaining with both anti-FLAG (Fig. 7A) and anti-Ripply2 antibodies (Fig. 12).

I conducted triple-immunostaining analysis of WT and *FLAG-Ripply2* TG embryos using anti-Tbx6, anti-Mesp2, and anti-Ripply2 antibodies. The segmentation cycle of embryos was determined by the oscillation pattern of Notch signaling activity (Fig. 12A a, f, and k), and the segmentation cycle was divided into stages I, II and III (Oginuma et al., 2008a). I found Ripply2 and Tbx6 to be predominantly colocalized in the nucleus (Fig. 12A b), suggesting a possible Tbx6–Ripply2 interaction. The confocal immunofluorescence data were further analyzed by grid-based methods (Fig. 12A e, j, o; B e, j, o; C).

During phase I of the segmentation cycle in control embryos, Ripply2-expressing cells formed a clear stripe at S-1, which overlapped with the Mesp2 stripe (Fig. 12A c). The Mesp2 and Ripply2 stripes shared the anterior limit with that of Tbx6 (Fig. 12A b, d, and e). The locations of Mesp2 and Ripply2 were still posterior to the Tbx6 anterior limit, which itself showed reduced Tbx6 signal (Fig. 12A e). In contrast with Mesp2-Tbx6 double-positive cells, which occasionally exhibited strong Tbx6 signal (Fig. 12A d), the Ripply2-Tbx6 double-positive cells showed a lower signal of both Ripply2 and Tbx6 (Fig. 12A b). In *FLAG-Ripply2* embryos a stronger Ripply2 signal than WT was detected (Fig. 12B b, c). Further, the number of Ripply2-Tbx6 double-positive cells in these embryos were fewer than in control (Fig. 12B b, arrow), and the Mesp2 intensity was low as compared to that in WT (Fig. 12B c, d). In some cases, the Mesp2 and Ripply2 locations were anterior to the Tbx6 anterior limit (Fig. 12B e).

During phase II, the Tbx6 signal in control was absent from the Mesp2-Ripply2 domain in the anterior PSM, its anterior limit regressed posteriorly, and was consistent with the posterior

boundary of Ripply2 (Fig. 12A h, i). The locations of Mesp2 and Ripply2 signals were anterior to the Tbx6 anterior limit (Fig. 12A j). Much of the Ripply2 protein was localized in Mesp2-expressing cells (Fig. 12A h). Only a small amount of Tbx6 signal was detected in the Ripply2-positive cells (Fig. 12A g arrow). In the *Flag-Ripply2* embryos, Ripply2 S-1 stripe showed a sharp posterior limit that corresponded to the anterior limit of the Tbx6-expressing domain (Fig. 12B g), as observed in control embryos. Interestingly, Mesp2 was almost undetectable in this phase (Fig. 12B h, j) and hence, hardly recognized in kernel density estimation (Fig. 12B j). This was significantly different from that of control embryos, in which Mesp2 was clearly observed during this phase (Fig. 12A h, j). FLAG-Ripply2 perhaps accelerated the down-regulation of Tbx6, which in turn lowered Mesp2 expression.

I detected two Mesp2 stripes in the control during phase III of the segmentation cycle (Fig. 12A m, n, and o). A new Mesp2 (S-1) stripe was in the anterior region of the Tbx6 domain, while the previous stripe observed in S0 overlapped with the Ripply2 stripe (Fig. 12A m, n). In *FLAG-Ripply2* TG embryos, I found several Ripply2 stripes in the PSM and somites (Fig. 12B l, m), indicating the prolonged expression of FLAG-Ripply2. On the other hand, the Mesp2 stripe in S0 remained only as a weak S-1 stripe (Fig. 12B m, o). In most embryos the Mesp2 signal appeared scattered in the Tbx6-expressing domain and no longer appeared as two stripes seen in the control (Fig. 12B m, n).

Quantitative analysis of the images from immunofluorescence studies confirmed the occurrence of several features proposed by qualitative studies. For quantification, all data sets were first classified based on their Mesp2 expression patterns, which revealed three patterns (Fig. 13); a single summit on the posterior (pattern 1) or anterior (pattern 2) side or two summits on both sides (pattern 3) of the Tbx6 anterior limit. Pattern 2 can be regarded as the end of Tbx6 anterior limit regression. In control embryos, the three spatial patterns corresponded with the three phases, which were determined by NICD expression pattern (Fig. 12A e, j, and o; Fig. 13). On the contrary, the

spatial patterns observed in *FLAG-Ripply2* embryos tend to correspond to pattern 2, including partial samples from phases I and III. The elevation in proportion of pattern 2 during phase I indicated that Ripply2 overexpression changed the position of Tbx6 anterior limit posteriorly *via* Tbx6 suppression. The estimated locations of Mesp2 and Ripply2 expression stripes were at intervals 68.23 μm and 60.49 μm, respectively (Fig. 12C). Further, the estimated location of Mesp2 always shifted rostrally to that of Ripply2 in control (Fig. 12C). The extent of these shifts was small but considerably stable throughout the phases (4.07 μm at pattern 1, 4.77 μm at pattern 2, and 2.32 μm at pattern 3) (Fig. 13). Despite the aberrant expression pattern of Ripply2 in *FLAG-Ripply2* embryos, their estimated locations of Mesp2 stripe were identical to those in control (Fig. 12C). This was illustrated by the Mesp2 stripe locations in pattern 2 (−34.53 μm in control and −34.30 μm in *FLAG-Ripply2*) (Fig. 13). This finding indicated that Ripply2 overexpression influenced only its signal strength but not the position of *Mesp2* expression. *FLAG-Ripply2* mice also showed Ripply2 expression in a region where somite formation was complete, an event never observed in control (Fig. 12C). The interval between its genuine expression (32.51 μm) coincided with that of Mesp2, and the position of remnant expression (−87.61 μm) in *FLAG-Ripply2* embryos (55.10 μm) was very close to that of Ripply2 stripes in patterns 1 and 2 (55.56 μm) in control (Fig. 13). This observation implies that the new Tbx6 anterior limit always appeared at a position ~55 μm posterior to its present position.

Scatter plot of control embryos showed that high Tbx6 intensity (>0.3) could be detected in the Ripply2 stripe in pattern-1 (Fig. 14B, left blue dot) of Ripply2$^{negative}$ group but not in Ripply2$^{high}$ group. Notably, Ripply2$^{low}$ group (intensity 0.07~0.3) exhibited lower Tbx6 levels compared to Ripply2$^{negative}$ group, indicating the Ripply2-mediated suppression of Tbx6 in the former (Fig. 12A b, arrow; Fig. 14B, left). When Ripply2 intensity was below 0.2, Tbx6 levels negatively correlated with Ripply2 levels (Fig. 14C, left). The cells in the Mesp2 S-1 domain of embryos showing pattern-3 (Fig. 14B, right blue dot) were not affected by presence of Ripply2. I observed Tbx6$^{high}$ cells in both

Mesp2$^{low}$ (intensity 0.1~0.3) and Mesp2$^{high}$ (intensity > 0.3) groups; the intensity of Tbx6 in these two groups were comparable (Fig. 14B. right). Taken together, these findings suggest that Tbx6 intensity is not influenced by the presence of Mesp2 (Fig. 14C, right).

The pattern of protein expression in *FLAG-Ripply2*;*Ripply2*-null embryos resembled that of *FLAG-Ripply2* embryos; Ripply2 was usually expressed as two or more stripes in both types of embryos (Fig. 7E, F). Unlike *Ripply2*-null samples, where the Tbx6 domain crossed over the Mesp2 domain (Fig. 7D), the Tbx6 domain was restricted to the posterior PSM in *FLAG-Ripply2*;*Ripply2*-null embryos (Fig. 7E, G). Further, the level of Mesp2 in these embryos was much lower than that in *Ripply2*-null embryos (Fig. 7F, G). These results indicate that the phenotype and rostro-caudal pattern of *FLAG-Ripply2*;*Ripply2*-null embryos differed from that of *Ripply2*-null embryos but resembled *FLAG-Ripply2* embryos owing to an increase in Ripply2 levels. Therefore, Ripply2 dosage might be important for somitogenesis.

In *FLAG-Ripply2* TG mice, although *Mesp2* mRNA and protein expression were restricted, Tbx6 expression was suppressed successfully and showed a normal anterior boundary as found in control embryos, suggesting the absence of Mesp2 involvement in Tbx6 suppression. Some of the *FLAG-Ripply2* samples exhibited spatial pattern-2 during phase I, indicating accelerated Tbx6 degradation despite of the reduction in Mesp2 level. This finding supports the claim that Ripply2 has a more direct role in Tbx6 degradation than Mesp2.

**Anterior limit of Tbx6 protein domain was established in *Mesp2*$^{Ripply2/Ripply2}$ mice**

The endogenous expression pattern of Ripply2 and Mesp2 were similar. Although I have observed Ripply2-dependent Tbx6 suppression in the anterior PSM, I cannot exclude the possibility that Ripply2 and Mesp2 work in concert to effect this suppression (Hypothesis-2). To test this possibility, I generated a *Mesp2*$^{Ripply2/Ripply2}$ mouse by replacing *Mesp2* with *Ripply2*. I confirmed the expression

of Ripply2 in the absence of Mesp2 at the anterior PSM (Fig. 15M, N, Fig. 16 D and Fig. 17). In *Mesp2*$^{L/L}$ embryo (Fig. 15E, E') (functional *Mesp1/2* DKO mouse due to the effect of pgk-neo construct), Tbx6 protein expression was dramatically expanded (Fig. 15G, G', H, H') and Ripply2 was completely undetectable (Fig. 15F, F') (Takahashi et al., 2000). Tbx6 expansion was not observed in *Mesp2*$^{Ripply2/Ripply2}$ mice, and a clear anterior boundary of Tbx6 was created even in the absence of Mesp2 (Fig. 15O, P), as observed in WT (Fig. 15A-D). Compared with discrete reduction of Tbx6 protein in Ripply2 expression domain, *Tbx6* mRNA showed a gradient (Fig. 18B-D), indicating that the RNA reduction is caused by a passive mechanism rather an active elimination. This finding indicates that Ripply2, and not Mesp2, is required for the disappearance of Tbx6 protein. T, another T-box family factor, is expressed as a gradient in the PSM, with levels decreasing from tail-bud to anterior PSM (Fig. 19B). It has an anterior limit that is almost identical to that of Tbx6, exactly overlapping with posterior limit of Ripply2 (Fig. 19C), and showing increased expression in *Mesp2*$^{L/L}$ embryos (Fig. 19E). This overexpression was also suppressed in *Mesp2*$^{Ripply2/Ripply2}$ embryos (Fig. 19H), indicating that Ripply2-mediated negative regulation could be a general mechanism for T-box family proteins in the PSM.

Though Tbx6 boundary was created normally, segmented somites were never observed in these *Mesp2*$^{Ripply2/Ripply2}$ embryos. As observed in *Mesp2*$^{L/L}$ embryos, *Mesp2*$^{Ripply2/Ripply2}$ embryos exhibited disappeared *Tbx18* expression and expanded *Uncx4.1* expression domain (Fig. 16F, H), indicating a caudalized somite property. Skeleton samples of *Mesp2*$^{Ripply2/Ripply2}$ proved this caudalized phenotype by showing fused pedicles of vertebrae (Fig. 20), confirming the requirement of Mesp2 for somite segmentation and rostro-caudal polarity. Noticeably, another Mesp family transcriptional factor, Mesp1, was expressed in *Mesp2*$^{Ripply2/Ripply2}$ embryos (Fig. 16B and Fig.17). *Mesp2*$^{MCM/MCM}$ (Mesp2 single KO) mouse had segmented somites, which is probably due to the rescue by up-regulated *Mesp1* (Fig.16) (Takahashi et al., 2007); and expressed Ripply2 at a lower level compared to WT

(Fig. 15J), resulting in the mild expansion of Tbx6 protein (Fig. 15K). Based on these results, I speculate that Ripply2 is sufficient for establishing segmental border, while the later segmentation requires Mesp function.

**Ectopic Ripply2 influences development of paraxial mesoderm**

Tbx6 is presumed to have two major regulatory functions. Neural ectoderm and mesoderm share a common progenitor persisting through all stages of axis elongation (Tzouanacou et al., 2009). Besides the regulation of somite segmentation, Tbx6 was reported to be required for cells to choose between a mesodermal and a neuronal differentiation pathway during gastrulation, that means Tbx6 is essential for the specification of posterior paraxial mesoderm, and in its absence cells destined to form posterior somites differentiate along a neuronal pathway (Takemoto et al., 2011). Ectopic neural tubes were detected upon Tbx6 reduction (Chapman and Papaioannou, 1998). In order to clarify if Ripply2-mediated down-regulation of Tbx6 protein is an general event and not specific to the anterior PSM, I generated inducible *Ripply2*-expressing TG mice, in which loxP-flanked mRFP could be removed, and *FLAG-Ripply2* could be expressed under the control of the CAG promoter (Fig. 21A).

Without Cre recombinase, mRFP is expressed in the entire embryo (Fig. 21B, center). To avoid embryonic lethality, I conditionally induced *Ripply2* using the *T* promoter-driven Cre recombinase, which is expressed in the primitive streak (PS) and posterior PSM (Perantoni et al., 2005). Reporter analysis using *Rosa26*$^{mTmG/mTmG}$ mice shows that Cre activity (GFP) begins from E8.5 (Fig. 22A–D) (Muzumdar et al., 2007). Cross-sectional analysis revealed GFP expression in the paraxial mesoderm, lateral plate mesoderm, and ectoderm at E8.5 (Fig. 22E, F). This area included the Tbx6-expressing domain and some part of the Sox2-positive neural tube (Fig. 22G). Ectopic *Ripply2* expression was observed from E8.5 (Fig. 23C, D and Fig. 24) instead of the mRFP

expression in the posterior half of embryos when crossed the inducible line with *T-Cre* mice (Fig. 21B right). Expression of FLAG-Ripply2 was also verified by western blotting using anti-FLAG antibody (Fig. 25). Hereafter this TG mice is referred to as *T-Cre;FLAG-Ripply2*. The *T-Cre;FLAG-Ripply2* embryos lost their endogenous *Ripply2* stripe (Figs. 23C, D). Although the signal strength of ectopic *Ripply2* was weaker when compared with that of endogenous *Ripply2*, the total amount of *Ripply2* transcript in *T-Cre;FLAG-Ripply2* embryos was greatly increased compared to that in the control (Fig. 24A, B).

The *T-Cre;FLAG-Ripply2* embryos elongated normally until E9.5, but did not form posterior somites. The expression of *Uncx4.1* and *Dll1*, markers of caudal somitic compartments, was severely impaired, indicating obscure rostral-caudal patterning of somites along AP axis (Fig. 23G, H). Between E9.5 and 10.5, the mutants showed a thin PSM and an unsegmented caudal trunk and tail (Fig. 26F). Interestingly, a cross-section of the PSM region shows tube-shaped structures at a bilateral position flanking the axial neural tube (Fig. 26G–I). This phenotype resembled that of *Tbx6*-null mutant embryos, in which bilateral ectopic neural tubes develop at the expense of the paraxial mesoderm (Chapman and Papaioannou, 1998). This finding leads to the possibility of ectopic neural tube formation due to a reduction in Tbx6 level induced by the ectopic Ripply2 expression.

**Tbx6 was destabilized by ectopic Ripply2 expression**

I examined the contribution of Tbx6 reduction to the supernumerary neural tube development in *T-Cre;FLAG-Ripply2* embryos by using double immunohistochemistry with anti-Sox2 and anti-Tbx6 antibodies. The transcriptional factor Sox2 is considered a marker for neural primordial cells. Its expression in control embryos from E8.5 to E10.5 was confined to the neural plate and neural tube (Fig. 26B, C and Fig. 27A, E), and Tbx6 was expressed at the posterior PSM (Fig. 26D, E and 27B,

F). In the *T-Cre;FLAG-Ripply2* embryos, some of the cells in the paraxial mesodermal compartment underlying the neural plate expressed Sox2 at E8.5 (Fig. 27C, arrow). Tbx6 was not expressed in the expected PSM region beneath the neural plate/neural tube, but was detected at the marginal region (Fig. 27D). By the E9.5 stage, the Sox2-positive cells formed the circular tubes near the central neural tube (Fig. 27G arrows), and the surrounding paraxial mesoderm cells were reduced in number (Fig. 27G, H). At E10.5, the *T-Cre;FLAG-Ripply2* embryos had completely lost their Tbx6 signal (Fig. 26J-L); on the other hand, multiple rosettes of Sox2-possitive tissue appeared lateral to the central neural tube in these embryos (Fig. 26G-I). The expression of these molecular markers indicated differentiation of the paraxial tissue into neural tissue and not mesoderm. These results were further confirmed by RT-PCR analysis, which showed increased *Sox2* expression and decreased undifferentiated mesoderm marker *T* at E9.5 (Fig. 24A, B).

Whole mount immunostaining showed that the domain of Tbx6 expression in *T-Cre;FLAG-Ripply2* embryo was reduced to a few Tbx6-positive cells around the edge of the tail-bud (Fig. 28D, H). This pattern was in contrast to that found in the control embryos, where Tbx6 was uniformly expressed in the posterior PSM (Fig6. 28C, G). *Tbx6* mRNA were detected in both control and *T-Cre;FLAG-Ripply2* embryos at E8.5 (Fig. 28A, B), indicating that Tbx6 protein, but not mRNA, is affected by ectopic Ripply2 expression. *Mesp2* expression was undetectable in the *T-Cre;FLAG-Ripply2* embryos (Figs. 23K, L and Fig. 24A, B). This result confirmed that Tbx6 is down-regulated by Ripply2 and not Mesp2, and indicated that Ripply2 promotes the suppression of Tbx6 at the post-translational level. The *Tbx6* transcript disappeared from the E9.5 stage (Fig. 28F); RT-PCR findings suggested gradual reduction in *Tbx6* transcription from E8.5 to E9.5 stage (Fig. 24A, B). Interestingly, the expression of another T-box family transcription factor, T, was also affected by Ripply2 (Fig. 28L, P) at the post-translational level at E8.5 in *T-Cre;FLAG-Ripply2* embryos (Fig. 28J and Fig. 24A), in a manner similar to that of Tbx6. This suggests that besides

Tbx6, other T-box family factors are also destabilized *via* Ripply2, which is consistent with reports shown in zebrafish (Kawamura et al., 2008; Wanglar et al., 2014). Unlike *Tbx6*, mRNA of *T* was still observed at E9.5 (Fig. 28N), although at reduced levels (Fig. 24B). These results clearly showed that the destabilization of both Tbx6 and T protein was induced by ectopic *Ripply2* expression, suggesting a general post-translational repression of T-box proteins by Ripply2 (Fig. 29).

**Ripply2 directly interact with Tbx6 protein**

Even though *in vivo* data indicate that Ripply2 may degrade Tbx6 protein directly, I failed to reproduce the degradation *in vitro*, since Tbx6 was never degraded in cultured cells. There could be some factor(s) helping the degradation in vivo, but absent in cultured cells. Since protein-protein interaction must be essential although it may not be sufficient for degradation, I presumed that Tbx6 and Ripply2 protein must bind to each other. This idea is also supported by the report that Ripply family proteins have a conserved domain which can interact with T-box family protein (Kawamura et al., 2008).

To examine if Ripply2 can interact with Tbx6, I co-tansfected Myc-Ripply2 and FLAG-Tbx6 expression constructs into 293T cells. The potential interaction between Ripply2 and Tbx6 was analyzed by immunoprecipitation using anti-FLAG antibody followed by western blotting with anti-Myc antibody. The result showed strong association of FLAG-Tbx6 with Myc-Ripply2 in 293T cell lysates (Fig. 30B), indicating that Ripply2 may influence the function of Tbx6 by forming a complex with Tbx6. To further explore whether the association between these two proteins is direct, I carried out an *in vitro* GST pull-down assay using bacterially expressed GST-Tbx6 and $His_6$-Ripply2 fusion proteins. GST-Tbx6 fusion protein, but not GST alone, was able to pull down $His_6$-Ripply2, indicating that Tbx6 directly interacts with Ripply2 (Fig. 30C).

**Tbx6 protein has two Ripply2-binding sites in a T-box domain**

Considering that Ripply2 protein can bind to T-box, which is highly conserved among the T-box family proteins, I generated constructs which express FLAG modified T-box (FLAG-T-box) and T-box deleted Tbx6 (FLAG-Tbx6$_{\Delta T\text{-box}}$). I found that the T-box domain alone is sufficient for the association with Ripply2 and that other regions of Tbx6 are dispensable for the interaction (Fig. 30B).

To identify the region of T-box involved in Ripply2 binding, I generated several kinds of deletion form of Tbx6 protein and performed co-immunoprecipitation assay with Ripply2. When C-terminal from amino acid 124 (Tbx6$_{1\sim124aa}$) or N-terminal up to amino acid 253 (Tbx6$_{253\sim436aa)}$, were deleted from Tbx6, those failed in binding with Ripply2 (Fig. 30B). Tbx6$_{1\sim152aa}$ and Tbx6$_{238\sim436aa}$ succeeded in Ripply2-interaction (Fig. 30B), suggesting that Tbx6 has two Ripply2-binding domains: amino acids 124~152 and 238~253. I further found that solo deletion in either 124~152aa (Tbx6$_{\Delta124\sim152}$) or 238~253 did not affect the ability to form complex with Ripply2 (Fig. 30B, C), indicating that each binding region can interact with Ripply2 protein independently. This idea was verified by the fact that Tbx6$_{\Delta124\sim152,\ \Delta238\sim253}$ abolished its ability to form complex with Ripply2 (Fig. 30B). Failure in pull down of His-Ripply2 by GST- Tbx6$_{\Delta124\sim152,\ \Delta238\sim253}$ indicated that the binding occurs through the two amino acid domains (Fig. 30C), whereas deletion of either 124~152 aa or 238~253aa had little effect.

**Ripply2 homology domain is required for the interaction with Tbx6**

I next generated mutant constructs for Ripply2. Ripply2 has two distinct motives; one is a so-called Ripply homology domain FPIQ and Groucho interacting domain WRPW. Deletion of Ripply homology domain (Myc-Ripply2$_{\Delta FPIQ}$) resulted in failure of making a Ripply2-Tbx6 complex (Fig. 31C), indicating that this conserved sequence is required for Ripply-mediated Tbx6 suppression.

Therefore, the T-box domain in Tbx6 and FPIQ motif in Ripply2 are indispensable for interactions between Tbx6 and Ripply2. The WRPW tetrapeptide motif, another important highly conservative domain, has been implicated in interaction with the transcriptional co-repressor Groucho/TLE in *Xenopus* Bowline and zebrafish Ripply1 (Kawamura et al., 2005; Kondow et al., 2006). I confirmed that WRPW-tetrapeptide motif is necessary to form Ripply2-Groucho complex using FLAG-TLE1/2, two kinds of homolog of Groucho/TLE family factors, to co-precipitate Myc-Ripply2 and Myc-Ripply2$_{\Delta WRPW}$. As expected, FLAG-TLE1 and FLAG-TLE2 precipitated Ripply2 but not Ripply2$_{\Delta WRPW}$, suggesting mouse Ripply2 can also repress the transcriptional activity of Tbx6 by working together with Groucho co-repressor as other animals (Fig. 31B).

## Discussion

In this study, I clarified relationships among three important transcription factors, Tbx6, Mesp2 and Ripply2 in somitogenesis. I found that the anterior limit of Tbx6 expression domain, which indicates the segmental border, is established by Ripply2 without the function of Mesp2. However, Mesp2 is required for the following somite segregation, which is a different event from positioning of the segmental border. In addition, ectopic Ripply2 expression in the entire PSM induces ectopic neurogenesis via suppressing T-box family factors, Tbx6 and T through a posttranslational process.

**Overexpression of Ripply2 influences spatial patterns of three factors during somitogenesis**

Through this study, I succeeded for the first time in visualizing the spatio-temporal transition process of three crucial factors, Tbx6, Mesp2, and Ripply2, in the anterior PSM. Regulation of somitogenesis by the 'segmentation clock' involves temporal oscillations in the cellular protein expression state. Using image-processing methods, I determined these dynamic changes in a comprehensive and quantitative manner. Each somatic cycle involves temporally regulated steps of Mesp2 expression (phase III), Ripply2 expression (phase I), and Tbx6 degradation (phase II). In control embryos, Mesp2 showed a clear stripe inside the Tbx6 domain at phase III; however, Tbx6 expression around its anterior limit did not show a concomitant reduction. Only Ripply2 expression at this anterior domain during phase I reduced the strength of Tbx6 signal. This finding indicates that Ripply2, and not Mesp2, regulates Tbx6 degradation.

Based on the Mesp2 expression pattern, I classified the quantitative image data into three patterns, which corresponded with phases I–III in control. The patterns observed in *Flag-Ripply2* were predominantly pattern-2. During phase I in control, Mesp2 and Ripply2 were colocalized at the region posterior to the Tbx6 anterior limit. However, Tbx6 anterior limit in *FLAG-Ripply2* was posterior to Mesp2 and Ripply2 peak. As a result, some samples in phase I also exhibits pattern-2. Phase III samples could also exhibit pattern-2 because the very low-intensity Mesp2 signal in S-1 of

*FLAG-Ripply2* sample might remain undetectable during phase III. These factors together contribute the predominance of pattern-2 in *FLAG-Ripply2* samples.

Reduction in Mesp2 might have also affected Notch activity in *FLAG-Ripply2* TG mice by activating Lunatic fringe (Lfng) (Morimoto et al., 2005). However, in this study, I did not observe any change in the two-hour somitogenic cycle. I calculated somite number in control (n = 3) and *FLAG-Ripply2* (n = 3) at E10.5 and found that the mean somites numbers in the *FLAG-Ripply2* (39.0) and control (39.7) embryos in the same litter did not differ significantly. Therefore, I conclude that Ripply2 overexpression alters the protein profile during the three phases in every cycle but not the duration of the somitogenic cycle.

**Ripply2 can rescue the Tbx6 anterior limit but not segmentation**

Somite was never observed in *Mesp2*$^{Ripply2/Ripply2}$ embryos, although the Tbx6 limit, which decides segmental border, was evident. Segmentation failure in *Mesp2*$^{Ripply2/Ripply2}$ embryos is similar to a phenotype obtained by the deficiency of *Mesp1/2* rather the KO of solo *Mesp2* (*Mesp2*$^{MCM/MCM}$). The up-regulation of *Mesp1* in *Mesp2*$^{MCM/MCM}$, which rescued segmentation, did not occur in *Mesp2*$^{Ripply2/Ripply2}$, suggesting that Mesp family factors are required for segmentation. Although *Mesp1* expression was detected in *Mesp2*$^{Ripply2/Ripply2}$ embryos, the expression level of *Mesp1* was not higher compared with WT (RT-PCR), indicating Ripply2 repressed *Mesp1* expression via Tbx6 elimination (Christiaen et al., 2009; Davidson et al., 2005). Thus, I propose that positioning of segmental border and subsequent segregation of somite boundaries are two important and consecutive events; the former is regulated by Ripply2, and the later is mainly regulated by Mesp factors.

**Revisiting the mechanism of rostral-caudal patterning**

After somites separate from the PSM, somites can be subdivided into rostral and the caudal compartments (Keynes and Stern, 1988). This subdivision provides a scaffold for the future vertebrae, which are formed by the fusion of the caudal part of a somite with the rostral part of the consecutive one (Aoyama and Asamoto, 2000; Bagnall et al., 1988; Goldstein and Kalcheim, 1992). Dll1-dependent Notch signaling (required for caudal identity) and its negative regulation via Mesp2 (required for rostral identity) is essential for the establishment of the rostro-caudal segment polarity (Oginuma et al., 2010; Takahashi et al., 2003). In *FLAG-Ripply2* embryos, the down-regulation of Tbx6 may affect rostro-caudal patterning, because the expression of both *Dll1* (Hofmann et al., 2004; White and Chapman, 2005) and *Mesp2* (Yasuhiko et al., 2006) depend on Tbx6. *Dll1* is expressed in the PSM and the posterior compartment of somites, and induces *Uncx4.1* which is required for the formation the vertebral component derived from caudal part of somites (Mansouri et al., 2000), while *Mesp2* is expressed in the rostral compartment and contribute to the establishment of the rostral property by suppressing *Dll1*expresion and also Notch signaling (Sasaki et al., 2011; Takahashi et al., 2000). Therefore, if the Tbx6-Dll1-Uncx4.1 pathway has a main function in rostro-caudal patterning, *Dll1* and *Uncx4.1* transcripts were expected to be enhanced associated with a caudalized phenotype. However, in *FLAG-Ripply2* mice exhibiting caudalized phenotype, neither *Dll1* nor *Uncx4.1* RNA expression was down-regulated, even though Tbx6 expression is greatly reduced. Further, *Ripply2*-null showed down-regulated *Dll1* and *Uncx4.1,* despite of strongly expanded Tbx6 (Morimoto et al., 2007), indicating that Tbx6 is not sufficient for inducing *Dll1*. Noticeably, *Mesp2* transcript and protein were also down-regulated in accordance with Tbx6 suppression. Mesp2 suppresses Notch activity via the activation of *Lfng*, which might function as a negative regulator of Notch signaling (Morimoto et al., 2005). In addition, Mesp2 acts as a transcriptional activator of *Epha4* in the anterior PSM (Nakajima et al., 2006). Mesp2 is also known to be a strong suppressor of genes such as *Dll1* and *Uncx4.1* which confer caudal properties upon the

somitic cells via Notch signaling (Takahashi et al., 2000). This is consistent with the caudalized phenotype of *FLAG-Ripply2* mice, which also exhibited reduced rostral marker *Tbx18* expression. These observations strongly support the idea that Mesp2 rather than Tbx6-Dll1 pathway has a main function in rostro-caudal patterning determination.

**Ripply2 down-regulates the T-box family factors in the PSM at the post-translational level**

I observed significant reduction in levels of both Tbx6 and T proteins in *T-Cre;FLAG-Ripply2* embryos, suggesting that T-box-containing proteins share properties that allow for negative regulation by Ripply2. However, I also noticed a difference in mRNA stability between *Tbx6* and *T*; the mRNA of the latter being long-lived. *T* expression, which was typically expressed in undifferentiated mesoderm cells, showed the level identical to that in control at E8.5 indicated that mesoderm population still existed in *T-Cre;FLAG-Ripply2*. Since T is known as an up-stream factor of Tbx6 (Chapman et al., 1996), and T protein was immediately affected by ectopic Ripply2, the reduction of Tbx6 at E8.5 could be a result of reduced T activity. Besides transcriptional down-regulation, Tbx6 level is also regulated at the post-translational level given that *Tbx6* mRNA lasts longer than the protein. Therefore, I speculate that the mechanism of negative regulation differs between these two T-box factors. T is predominently regulated at the post-translational level, while Tbx6 is regulated at both post-transcriptional and post-translational level in differentiating mesoderm.

**Ripply2 protein interacts with Tbx6 protein**

The overlapping expression of Ripply and T-box genes observed in various developing tissues and organs (A. Kawamura and S. Takada) supports the idea that the two proteins cooperate during development. In zebrafish, it is reported that Ripply homology domain processes the ability for tbx6

binding, and T-box alone, which is highly conserved among the Tbx family proteins, is sufficient for the association with ripply (Kawamura et al., 2008). Observations in my study showed that mouse T-box domain is sufficient for Ripply2-binding, and tetrapeptide FPIQ in the Ripply homology domain is essential for the interaction with Tbx6. These results are consistent with that observed in zebrafish. Two domains in the T-box: 124~152aa and 238~253aa are identified as binding sites for Ripply2. Both of these two areas are highly conserved in T-box family proteins; they are located in two β-sheets in the special structures individually, which allow them to pinch Ripply protein like a clip. In order to fully investigate Tbx6 and Ripply2 function, we still need further deletion experiments in vivo.

**The conserved mechanism of Ripply-mediated Tbx6 down-regulation among vertebrates**

Ripply2 is required for the termination of *Mesp2* expression at an appropriate time to prevent prolonged Mesp2 activity in the subsequent cycle of somitogenesis. Zebrafish and *Xenopus* Ripply-family factors also display similar repressor functions on *mesp* expression (Kawamura et al., 2005; Kawamura et al., 2008; Kondow et al., 2007). In zebrafish and *Xenopus*, as previously reported, the suppression is achieved by recruitment of the Groucho co-repressor *via* the WRPW motif and its association with the T-box, which blocks the Tbx6 transcriptional activity required for *mesp* induction. Interaction analyses in my work also showed the Groucho/TLE-mRipply2 binding. Although the Groucho homologs TLE1 and TLE3 are expressed in mouse PSM, their function in mouse embryo has not been validated. Functional analysis for Ripply2$_{\Delta WRPW}$ in vivo may be helpful in understanding of the role of Groucho/TLE in segmental border decision. Despite zebrafish ripply1 is reported to inhibit tbx6 transcriptional activation in reporter assay, it is not confirmed as a main process for tbx6 suppression in vivo. Recently, zebrafish tbx6 protein has been found to be degraded by ripply1/2 (Wanglar et al., 2014). I also showed that post-translational regulation via Ripply2 is

necessary for Tbx6 function, supporting that post-translational degradation is probably a general negative regulation mechanism among vertebrates.

Though it is already known that mouse Tbx6 is degraded in an ubiquitin-dependent manner in the PSM (Oginuma et al., 2008b), the destabilization of Tbx6 cannot be attributed only to Ripply2. It has been found that Tbx6 is not degraded by Ripply2 in cultured cells (unpublished data), indicating existence of other factor(s) involved in Tbx6 down-regulation in vivo. Furthermore, Ripply family members have never been reported to be directly involved in protein degradation. One possibility is that Ripply2 is an indirect factor, and induces Tbx6 degradation via acting as a transcriptional regulator on some down-stream factor(s). Spatio-temporal analysis of WT samples showed that Tbx6 was degraded during phase I after Ripply2 expression was observed. Taking the length of every phase into account, Tbx6 must be suppressed within about 40 minutes. If that is the case, Ripply2 has to regulate the expression of other factor(s) within a very short period of time during every somitic cycle. The most plausible possibility is that Ripply2 lead Tbx6 degradation via guiding the interaction between Tbx6 and PSM specific ubiquitin ligase. The identification of an E3 ubiquitin ligase specific to Tbx6 *via* extensive molecular analysis of the ubiquitin-mediated protein degradation pathway will help in elucidating the mechanism of this complex and sophisticated segmentation program.

# Materials and Methods

**Animals**

The wild-type (WT) mice used in this study are MCH (a closed colony established at CLEA, Japan). The *Ripply2*-null, *Mesp2*$^{L/L}$ (Takahashi et al., 2000) and *Mesp2*$^{MCM/MCM}$ (Takahashi et al., 2007) mice were established and maintained in the animal facility of the National Institute of Genetics, Japan (Morimoto et al., 2007). Ripply2 over-expressing transgenic mouse was generated by injecting transgene composed of putative *Ripply2* enhancer and promoter (Dunty et al., 2008; Morimoto et al., 2007) with *Ripply2* cDNA and SV40 poly A signal into fertilized eggs (Supplementary Fig. 2A). For ectopic expression of *Ripply2, a transgenic mouse expressing CAG*-floxed *lyn-mRFP fused with FLAG-Ripply2* was generated and crossed with a *T-Cre* mice (Perantoni et al., 2005). Rosa26$^{mTmG}$ mice (Muzumdar et al., 2007) were obtained from the Jackson Laboratory. Noon on the day of the copulation plug was defined as embryonic day (E) 0.5.

**Targeting strategy to generate Ripply2 knock-in mice**

*Ripply2* cDNA was inserted in the pCMV7.1 to make *3xFLAG* modified *Ripply2* cDNA. To construct a knockin vector, a 7-kb genomic DNA fragment of the 5' upstream region of *Mesp2*, referred as HB-6.0 previously (Takahashi et al., 2000), was ligated in-frame in the XhoI site located in *FLAG-Ripply2* cDNA (HB-*FLAG-Ripply2*). Then, the HB-*FLAG-Ripply2* was inserted in the floxed *pgk-neo* cassette with a 1-kb XbaI-fragment of short arm and *pgk-DT* cassette used previously (Saga et al., 1997). These vectors were linearized and introduced into TT2 ES cells (C57BL/6 (B6)/CBA) as described (Yagi et al., 1993). After selection using G418, resistant clones were isolated and their DNA was analyzed by PCR using a neo-specific primer, *NeoAL2* (5'−GAAAGAACCAGCTGGGGCTCGAG−3'), and a *Mesp2* genomic primer, *HLH-R3* (5'−GGAAGTTGAGTTCCTCATCACGATC−3'). Correct homologous recombinants were used for aggregation with MCH 8-cells and then blastcysts were transferred to pseudopregnant female

recipients. The resulting chimeric mice were bred with MCH females. Germline transmission of the targeted allele was confirmed by PCR.

**Whole-mount in situ hybridization**

The InsituPro system (M&S Instruments) was used for whole-mount in situ hybridization according to the manufacturer's instructions. The probes used in this study were prepared as described previously (Morimoto et al., 2007; Nomura-Kitabayashi et al., 2002; Takahashi et al., 2003; Takahashi et al., 2000; Yasuhiko et al., 2006).

**Real-time PCR**

For RT-PCR analysis, presomitic mesoderm was dissected individually from embryos at E8.5, E9.5 and E10.5, and total RNA was prepared according to the method described before (Saga et al., 1996). One microgram total RNA was used for reverse transcription reaction with SuperscriptIII (Invitrogen) and oligo-dT primer. To distinguish between the transcripts derived from endogenous *Ripply2*, *Mesp1*, *Mesp2*, *Tbx6*, *T (brachyury)* and *Sox2*, the following specific pairs of primers were used, respectively.

*Ripply2*:F (5′- ATGGATACCACCGAGAGCGCCGAGA -3′) and R (5′-GGTACCCGGGCTGCGCGGAC-3′); *Mesp1*: F (5′- CCTTCGGAGGGAGTAGATC-3′) and R (5′-AAAGCTTGTGCCTGCTTCA-3′); *Mesp2*: F (5′- GACTGGACACTGGACACAATCCACT-3′) and R (5′-GGCCATAGCCAAGCAGACCTCAAA-3′); *Tbx6*: F (5′-AGGCCCGCTACTTGTTTCTTCTGG-3′) and R (5′- TGGCTGCATAGTTGGGTGGCTCTC-3′); *T*: F (5′-ATCAGAGTCCTTTGCTAGGTAG-3′) and R (5′-GTTACAATCTTCTGGCTATGC-3′)

*Sox2*:F (5′-GCGGAGTGGAAACTTTTGTCC-3′) and R (5′-CGGGAAGCGTGTACTTATCCTT-3′); *G3PDH*:F (5′-ACCACAGTCCATGCCATCAC-3′) and R (5′-TCCACCACCCTGTTGCTGTA-3′). The housekeeping *G3PDH* gene was used as "reference" gene. PCR reactions were carried out in 96-well microtiter plates in a 20 μl reaction volume with KAPA SYBR® FAST Universal 2X qPCR Master Mix (KAPA BIOSYSTEMS) with optimized concentrations of specific primers. A Thermal Cycler Dice Real Time System (TAKARA) was programmed for an initial step of 10s at 94°C, followed by 39 thermal cycles of 15s at 94°C, 15s at 60°C, 30s at 72°C. A 1:25 dilution of each cDNA was used as template in real-time PCR. Specificity of PCR amplification of each primer pair was confirmed by melting curve analysis (Ririe et al., 1997). Standard curves were generated by measuring threshold cycle (CT) values of ten-fold serial dilutions of the calibrator cDNAs. The relative transcript level was determined by a method and formula as described (Pfaffl, 2001).

**Generation of anti-Ripply2 antibody**

His-tagged fragments of Ripply2 protein (full Ripply2 antigen) (White and Chapman, 2005) were produced using the pCold system (Takara) and Escherichia coli strain BL21(DE3) as a host strain. The Ripply2 fragments were extracted from bacterial culture using the TALON Metal Affinity Resin (Clontech), and dialysis using a semipermeable membrane cassette (Pierce), followed by Vivaspin column concentration (GE). Rabbits (two animals) and guinea pig (two animals) were immunized with the purified Ripply2 fragments and processed for antibody purification following the standard procedures of Hokudo Bio (Abuta, Hokkaido, Japan).

**Whole-mount immunohistochemistry**

For whole-mount detection of Ripply2, Tbx6 or Brachyury, embryos were fixed with 4% paraformaldehyde (PFA) in PBS overnight at 4°C, incubated with guinea pig anti-Ripply2 (1:50), rabbit anti-Tbx6 (1:200) or goat anti-Brachyury (1:200) antibodies, followed by Alexa-488-conjugated goat anti-guinea pig IgG (1:200), Alexa-594-conjugated donkey anti-rabbit IgG (1:200) or Alexa-594-conjugated donkey anti-goat IgG (1:200). For double immunostaining, samples were incubated with mouse anti-FLAG (1:5000) and rabbit anti-Tbx6, then incubated with Alexa-488-conjugated donkey anti-mouse IgG (1:200) and Alexa-594-conjugated donkey anti-rabbit IgG (1:200). Samples were observed using a confocal microscope (Olympus FV1200 IX83).

**Section immunohistochemistry**

Mouse embryo and tail samples were fixed in 4% PFA, embedded in OCT compound and frozen in liquid nitrogen. Frozen sections (7 μm) were immersed in antigen unmasking solution (Vector Laboratories) and autoclaved at 105°C for 15 minutes. The detection of FLAG was performed by incubation with anti-FLAG (1:10000, Sigma) antibody, followed by incubation with Alexa-488-conjugated donkey anti-mouse antibody (1:250, life technologies). The detection of NICD or Mesp2 was performed by incubation with anti-active-NICD (1:1000, Cell Signaling Technology) or anti-Mesp2 (1:400) antibodies, respectively, followed by incubation with horseradish peroxidase (HRP)–conjugated donkey anti-rabbit IgG (1:200, Amersham Pharmacia Biotech) and treatment with Cyanin 3 tyramid. For tri-immunohistochemistry of Ripply2, Mesp2 and Tbx6, anti-Mesp2 (1:400) were used, followed by incubation with HRP-conjugated donkey anti-rabbit IgG (1:1000, Cell Signaling) and treatment of Cyanin 3 tyramid. Then the same slides were applied by anti-Ripply2 (1:100) or anti-Tbx6 (1:200) antibodies, followed by Alexa-488-conjugated goat anti-guinea pig IgG or Alexa-647-conjugated donkey anti-rabbit IgG

(1:250, life technologies). For the detection of Sox2 or Tbx6, slides were incubated with anti-Sox2 (1:200, Cell Signaling Technology) or anti-Tbx6 (1:200) antibodies, followed by incubation with Alexa-594-conjugated donkey anti-Goat IgG (1:250, life technologies) and Alexa-647-conjugated donkey anti-rabbit IgG (1:250, life technologies).

**Grid-based quantitative image processing**

The confocal fluorescent images (Tbx6, Mesp2, Ripply2 and DAPI) were processed using statistics language R (3.1.0 and later) running on an IDE (RStudio 0.98.953 and later) with some packages (RImageBook, EBImage, biOps, MASS, signal, TTR, xts, zoo, mgcv). The image is divided into an array of 10-by-10 pixel (2.67-by-2.67 μm) grids then median intensity of each 100-pixel grid is attributed as representative fluorescent intensity of the gird. Alignment of expression anterior limit of Tbx6 is determined as follows. The Tbx6 image was line-scanned from anterior to posterior of the tail to record series of numeric values of the fluorescent intensities (vector). Savitzky-Golay smoothing filter was then applied on the vector and the 3rd derivative of the smoothing vector was used for detecting location of significant rise of Tbx6 fluorescent intensities. First location of such intensities was plotted as Tbx6 expression anterior limit, and the anterior limit was obtained from an LM fitting of the plots. The distance of the 100-pixel grid is determined as shortest length from the centre of the grid to the anterior limit. In this way, the 4-image set is transformed to a data frame in which each row is consisted with 5 numerical values: distance in pixel and fluorescent intensities (0 to 1) of Tbx6, Mesp2, Ripply2 and DAPI. Relationships between the distance and the fluorescent intensities are defined using spline smoothing regression.

**Skeletal preparation**

Embryonic day 18.5 (E18.5) mouse embryos were fixed with 100% ethanol. For genotyping, PCR was performed using a piece of embryonic liver digested with proteinase K (Roche). Alcian Blue and Alizarin Red staining were performed as described (Saga et al., 1997; Takahashi et al., 2000).

**Immunoprecipitation**

HEK 293T cells, obtained from ATCC (Manassas, VA), were cultured in Dulbecco's modified Eagle's medium supplemented with 10% fetal bovine serum at 37 ° C under 5% CO2 at mosphere.

Cells were transiently transfected with PEI (Polyethylenimine) (polysciences,Inc) and constructs then incubated for 24 h before analysis. Cells were lysed in 50 mM Tris-HCl (pH 7.4), 150 mM NaCl, 1mM EDTA (pH 8.0), 0.5% Nonidet P-40, 1mM dithiothreitol (DTT), 7.5 mM b-glycerophosphate (Calbiochem), 0.1mM phenylmethylsulfonyl fluoride (PMSF) and 20mM MG132 (PEP Tide) mixture protein inhibitors. Immunoprecipitation were performed as described previously (Lou et al., 2006). The supernatants were then incubated with 10 µl of anti-FLAG M2 affinity gel (Sigma) on a rotator for 3 h at 4°C. After several washes, precipitates were boiled with 10 µl of 2×Sample buffer, separated by SDS-PAGE, and then subjected to western blotting analysis as described previously. Bound proteins were then eluted and subjected to Western blotting was performed using the primary antibodies Rabbit anti-myc antibody (1/5000, Sigma), mouse anti-FLAG (1/5000, Sigma) and mouse anti-β-tubulin (1:5000, Sigma). This was followed by incubation with goat anti-rabbit IgG conjugated with HRP (1:5000, cell signal) and donkey anti-mouse (Jackson) as the secondary antibody. .

**Western blotting**

Embryos and 293T culture cells were lysed with 50 mM Hepes (pH 7.4), 150 mM NaCl, 1mM

EDTA (pH 8.0), 1% Triton-100, 0.02% Sodium Deoxycolete, and 20mM MG132 (PEP Tide), and then sonicated with an ultrasonic processor (Vibra Cell, Sonics and Material Inc.). Each extracts were then resolved on 12.5% SDS-PAGE gels and electroblotted onto nitrocellulose membrane (BioTrace NT, Pall Corporation). The membrane was incubated with the primary antibodies, guinea pig anti-Ripply2 (1:1000), anti-myc (1:5000, Sigma), mouse anti-FLAG (1:5000, Sigma) and mouse anti-β-tubulin (1:5000, Sigma), followed by donkey anti-guinea pig-HRP, donkey anti Rabbit-HRP, or donkey anti mouse-HRP (1:5000, CHEMICON), respectively as secondary antibodies.

**GST Pull-down Assay**

Recombinant proteins expressed in Escherichia coli strain BL21(DE3) were induced with 1 mM isopropyl 1-thio-β-D-galactopyranoside for 16 h at 20 °C. The cells were collected, resuspended in lysis buffer (25 mM Hepes-KOH (pH 7.4), 150 mM NaCl, 1mM EDTA (pH 8.0), 0.1% Nonidet P-40, 1mM dithiothreitol (DTT), 0.1mM phenylmethylsulfonyl fluoride (PMSF) and 20mM MG132 (PEP Tide) mixture protein inhibitors), and sonicated. Purified His-Ripply2 protein was incubated with total lysates from Glutathione-S-transferase (GST) or GST-Tbx6 fusion protein-expressing E. coli cells for 1h, and then mixed with Glutathione-Sepharose beads (wet volume 60 μL; GE Healthcare Ltd.), rotating for 2 h. The beads were washed five times with washing buffer (25 mM Hepes-KOH (pH 7.4), 500 mM NaCl, 1mM EDTA (pH 8.0), 1% Nonidet P-40, and 1mM Dithiothreitol (DTT)). After eluted with 2xSDS loading buffer, beads were analyzed by 10% SDS–PAGE using anti-Ripply2 antibodies followed by staining with CBB R-250.

**Acknowledgments**

I thank Drs. Yumiko Saga, Rieko Ajima, and Youichirou Ninomiya for supporting my entire research. I thank member of Mammalian Development Laboratory for valuable suggestion and support. I am particularly thankful to Noriko Yamatani and Makoto Kiso (National Institute of Genetics, Japan) for generating the transgenic and knockin mice used in this study. I am grateful to Yukuto Yasuhiko for providing reagents. I thank Mark Lewandoski for generously providing the *T-Cre* mice. I am thankful to Astushi Suzuki for providing vector *pCold*. I am indebted to my family member, Mr. Rengui Zhao amd Mrs. Jianhui Fan for the economic and emotional supports. I am grateful to SHOSHI KAWASHIMA Memorial Schalorship Fundation, and JASSO Scholarship for the economic supports. This work was supported by funding from the Transdisciplinary Research Integration Center of the Research Organization of Information and Systems.

## Reference


Aoyama, H., Asamoto, K., 2000. The developmental fate of the rostral/caudal half of a somite for vertebra and rib formation: experimental confirmation of the resegmentation theory using chick-quail chimeras. Mech Dev. 99, 71-82.

Bagnall, K. M., Higgins, S. J., Sanders, E. J., 1988. The contribution made by a single somite to the vertebral column: experimental evidence in support of resegmentation using the chick-quail chimaera model. Development. 103, 69-85.

Bessho, Y., Hirata, H., Masamizu, Y., Kageyama, R., 2003. Periodic repression by the bHLH factor Hes7 is an essential mechanism for the somite segmentation clock. Genes Dev. 17, 1451-6.

Borycki, A. G., Emerson, C. P., Jr., 2000. Multiple tissue interactions and signal transduction pathways control somite myogenesis. Curr Top Dev Biol. 48, 165-224.

Brand-Saberi, B., Christ, B., 2000. Evolution and development of distinct cell lineages derived from somites. Curr Top Dev Biol. 48, 1-42.

Bussen, M., Petry, M., Schuster-Gossler, K., Leitges, M., Gossler, A., Kispert, A., 2004. The T-box transcription factor Tbx18 maintains the separation of anterior and posterior somite compartments. Genes Dev. 18, 1209-21.

Chan, T., Kondow, A., Hosoya, A., Hitachi, K., Yukita, A., Okabayashi, K., Nakamura, H., Ozawa, H., Kiyonari, H., Michiue, T., Ito, Y., Asashima, M., 2007. Ripply2 is essential for precise somite formation during mouse early development. FEBS Lett. 581, 2691-6.

Chan, T., Satow, R., Kitagawa, H., Kato, S., Asashima, M., 2006. Ledgerline, a novel Xenopus laevis gene, regulates differentiation of presomitic mesoderm during somitogenesis. Zoolog Sci. 23, 689-97.

Chapman, D. L., Agulnik, I., Hancock, S., Silver, L. M., Papaioannou, V. E., 1996. Tbx6, a mouse T-Box gene implicated in paraxial mesoderm formation at gastrulation. Dev Biol. 180, 534-42.

Chapman, D. L., Papaioannou, V. E., 1998. Three neural tubes in mouse embryos with mutations in the T-box gene Tbx6. Nature. 391, 695-7.

Christiaen, L., Stolfi, A., Davidson, B., Levine, M., 2009. Spatio-temporal intersection of Lhx3 and Tbx6 defines the cardiac field through synergistic activation of Mesp. Dev Biol. 328, 552-60.

Couly, G. F., Coltey, P. M., Le Douarin, N. M., 1993. The triple origin of skull in higher vertebrates: a study in quail-chick chimeras. Development. 117, 409-29.

Davidson, B., Shi, W., Levine, M., 2005. Uncoupling heart cell specification and migration in the simple chordate Ciona intestinalis. Development. 132, 4811-8.

Delfini, M. C., Dubrulle, J., Malapert, P., Chal, J., Pourquie, O., 2005. Control of the segmentation process by graded MAPK/ERK activation in the chick embryo. Proc Natl Acad Sci U S A. 102, 11343-8.

Diez del Corral, R., Olivera-Martinez, I., Goriely, A., Gale, E., Maden, M., Storey, K., 2003. Opposing FGF and retinoid pathways control ventral neural pattern, neuronal differentiation, and segmentation during body axis extension. Neuron. 40, 65-79.

Dubrulle, J., McGrew, M. J., Pourquie, O., 2001. FGF signaling controls somite boundary position and regulates segmentation clock control of spatiotemporal Hox gene activation. Cell. 106, 219-32.

Dunty, W. C., Jr., Biris, K. K., Chalamalasetty, R. B., Taketo, M. M., Lewandoski, M., Yamaguchi, T. P., 2008. Wnt3a/beta-catenin signaling controls posterior body development by coordinating mesoderm formation and segmentation. Development. 135, 85-94.

Goldstein, R. S., Kalcheim, C., 1992. Determination of epithelial half-somites in skeletal morphogenesis. Development. 116, 441-5.

Hitachi, K., Danno, H., Tazumi, S., Aihara, Y., Uchiyama, H., Okabayashi, K., Kondow, A., Asashima, M., 2009. The Xenopus Bowline/Ripply family proteins negatively regulate the transcriptional activity of T-box transcription factors. Int J Dev Biol. 53, 631-9.

Hofmann, M., Schuster-Gossler, K., Watabe-Rudolph, M., Aulehla, A., Herrmann, B. G., Gossler, A., 2004. WNT signaling, in synergy with T/TBX6, controls Notch signaling by regulating Dll1 expression in the presomitic mesoderm of mouse embryos. Genes Dev. 18, 2712-7.

Kawamura, A., Koshida, S., Hijikata, H., Ohbayashi, A., Kondoh, H., Takada, S., 2005. Groucho-associated transcriptional repressor ripply1 is required for proper transition from the presomitic mesoderm to somites. Dev Cell. 9, 735-44.

Kawamura, A., Koshida, S., Takada, S., 2008. Activator-to-repressor conversion of T-box transcription factors by the Ripply family of Groucho/TLE-associated mediators. Mol Cell Biol. 28, 3236-44.

Keynes, R. J., Stern, C. D., 1988. Mechanisms of vertebrate segmentation. Development. 103, 413-29.

Kondow, A., Hitachi, K., Ikegame, T., Asashima, M., 2006. Bowline, a novel protein localized to the presomitic mesoderm, interacts with Groucho/TLE in Xenopus. Int J Dev Biol. 50, 473-9.

Kondow, A., Hitachi, K., Okabayashi, K., Hayashi, N., Asashima, M., 2007. Bowline mediates association of the transcriptional corepressor XGrg-4 with Tbx6 during somitogenesis in Xenopus. Biochem Biophys Res Commun. 359, 959-64.

Kraus, F., Haenig, B., Kispert, A., 2001. Cloning and expression analysis of the mouse T-box gene Tbx18. Mech Dev. 100, 83-6.

Lou, X., Fang, P., Li, S., Hu, R. Y., Kuerner, K. M., Steinbeisser, H., Ding, X., 2006. Xenopus Tbx6 mediates posterior patterning via activation of Wnt and FGF signalling. Cell Res. 16, 771-9.

Mansouri, A., Voss, A. K., Thomas, T., Yokota, Y., Gruss, P., 2000. Uncx4.1 is required for the formation of the pedicles and proximal ribs and acts upstream of Pax9. Development. 127, 2251-8.

Monsoro-Burq, A. H., Le Douarin, N., 2000. Duality of molecular signaling involved in vertebral chondrogenesis. Curr Top Dev Biol. 48, 43-75.

Moreno, T. A., Kintner, C., 2004. Regulation of segmental patterning by retinoic acid signaling during Xenopus somitogenesis. Dev Cell. 6, 205-18.

Morimoto, M., Sasaki, N., Oginuma, M., Kiso, M., Igarashi, K., Aizaki, K., Kanno, J., Saga, Y., 2007. The negative regulation of Mesp2 by mouse Ripply2 is required to establish the rostro-caudal patterning within a somite. Development. 134, 1561-9.

Morimoto, M., Takahashi, Y., Endo, M., Saga, Y., 2005. The Mesp2 transcription factor establishes segmental borders by suppressing Notch activity. Nature. 435, 354-9.

Muzumdar, M. D., Tasic, B., Miyamichi, K., Li, L., Luo, L., 2007. A global double-fluorescent Cre reporter mouse. Genesis. 45, 593-605.

Nakajima, Y., Morimoto, M., Takahashi, Y., Koseki, H., Saga, Y., 2006. Identification of Epha4 enhancer required for segmental expression and the regulation by Mesp2. Development. 133, 2517-25.

Nomura-Kitabayashi, A., Takahashi, Y., Kitajima, S., Inoue, T., Takeda, H., Saga, Y., 2002. Hypomorphic Mesp allele distinguishes establishment of rostrocaudal polarity and segment border formation in somitogenesis. Development. 129, 2473-81.

Oginuma, M., Hirata, T., Saga, Y., 2008a. Identification of presomitic mesoderm (PSM)-specific Mesp1 enhancer and generation of a PSM-specific Mesp1/Mesp2-null mouse using BAC-based rescue technology. Mech Dev. 125, 432-40.

Oginuma, M., Niwa, Y., Chapman, D. L., Saga, Y., 2008b. Mesp2 and Tbx6 cooperatively create periodic patterns coupled with the clock machinery during mouse somitogenesis. Development. 135, 2555-62.

Oginuma, M., Takahashi, Y., Kitajima, S., Kiso, M., Kanno, J., Kimura, A., Saga, Y., 2010. The oscillation of Notch activation, but not its boundary, is required for somite

border formation and rostral-caudal patterning within a somite. Development. 137, 1515-22.

Perantoni, A. O., Timofeeva, O., Naillat, F., Richman, C., Pajni-Underwood, S., Wilson, C., Vainio, S., Dove, L. F., Lewandoski, M., 2005. Inactivation of FGF8 in early mesoderm reveals an essential role in kidney development. Development. 132, 3859-71.

Pfaffl, M. W., 2001. A new mathematical model for relative quantification in real-time RT-PCR. Nucleic Acids Res. 29, e45.

Ririe, K. M., Rasmussen, R. P., Wittwer, C. T., 1997. Product differentiation by analysis of DNA melting curves during the polymerase chain reaction. Anal Biochem. 245, 154-60.

Saga, Y., Hata, N., Kobayashi, S., Magnuson, T., Seldin, M. F., Taketo, M. M., 1996. MesP1: a novel basic helix-loop-helix protein expressed in the nascent mesodermal cells during mouse gastrulation. Development. 122, 2769-78.

Saga, Y., Hata, N., Koseki, H., Taketo, M. M., 1997. Mesp2: a novel mouse gene expressed in the presegmented mesoderm and essential for segmentation initiation. Genes Dev. 11, 1827-39.

Sasaki, N., Kiso, M., Kitagawa, M., Saga, Y., 2011. The repression of Notch signaling occurs via the destabilization of mastermind-like 1 by Mesp2 and is essential for somitogenesis. Development. 138, 55-64.

Sawada, A., Shinya, M., Jiang, Y. J., Kawakami, A., Kuroiwa, A., Takeda, H., 2001. Fgf/MAPK signalling is a crucial positional cue in somite boundary formation. Development. 128, 4873-80.

Takahashi, J., Ohbayashi, A., Oginuma, M., Saito, D., Mochizuki, A., Saga, Y., Takada, S., 2010. Analysis of Ripply1/2-deficient mouse embryos reveals a mechanism underlying the rostro-caudal patterning within a somite. Dev Biol. 342, 134-45.

Takahashi, Y., Inoue, T., Gossler, A., Saga, Y., 2003. Feedback loops comprising Dll1, Dll3 and Mesp2, and differential involvement of Psen1 are essential for rostrocaudal patterning of somites. Development. 130, 4259-68.

Takahashi, Y., Koizumi, K., Takagi, A., Kitajima, S., Inoue, T., Koseki, H., Saga, Y., 2000. Mesp2 initiates somite segmentation through the Notch signalling pathway. Nat Genet. 25, 390-6.

Takahashi, Y., Yasuhiko, Y., Kitajima, S., Kanno, J., Saga, Y., 2007. Appropriate suppression of Notch signaling by Mesp factors is essential for stripe pattern formation leading to segment boundary formation. Dev Biol. 304, 593-603.

Takemoto, T., Uchikawa, M., Yoshida, M., Bell, D. M., Lovell-Badge, R., Papaioannou, V. E.,

Kondoh, H., 2011. Tbx6-dependent Sox2 regulation determines neural or mesodermal fate in axial stem cells. Nature. 470, 394-8.

Tzouanacou, E., Wegener, A., Wymeersch, F. J., Wilson, V., Nicolas, J. F., 2009. Redefining the progression of lineage segregations during mammalian embryogenesis by clonal analysis. Dev Cell. 17, 365-76.

Wahl, M. B., Deng, C., Lewandoski, M., Pourquie, O., 2007. FGF signaling acts upstream of the NOTCH and WNT signaling pathways to control segmentation clock oscillations in mouse somitogenesis. Development. 134, 4033-41.

Wanglar, C., Takahashi, J., Yabe, T., Takada, S., 2014. Tbx protein level critical for clock-mediated somite positioning is regulated through interaction between Tbx and Ripply. PLoS One. 9, e107928.

White, P. H., Chapman, D. L., 2005. Dll1 is a downstream target of Tbx6 in the paraxial mesoderm. Genesis. 42, 193-202.

Yagi, T., Tokunaga, T., Furuta, Y., Nada, S., Yoshida, M., Tsukada, T., Saga, Y., Takeda, N., Ikawa, Y., Aizawa, S., 1993. A novel ES cell line, TT2, with high germline-differentiating potency. Anal Biochem. 214, 70-6.

Yasuhiko, Y., Haraguchi, S., Kitajima, S., Takahashi, Y., Kanno, J., Saga, Y., 2006. Tbx6-mediated Notch signaling controls somite-specific Mesp2 expression. Proc Natl Acad Sci U S A. 103, 3651-6.

# Figure 1

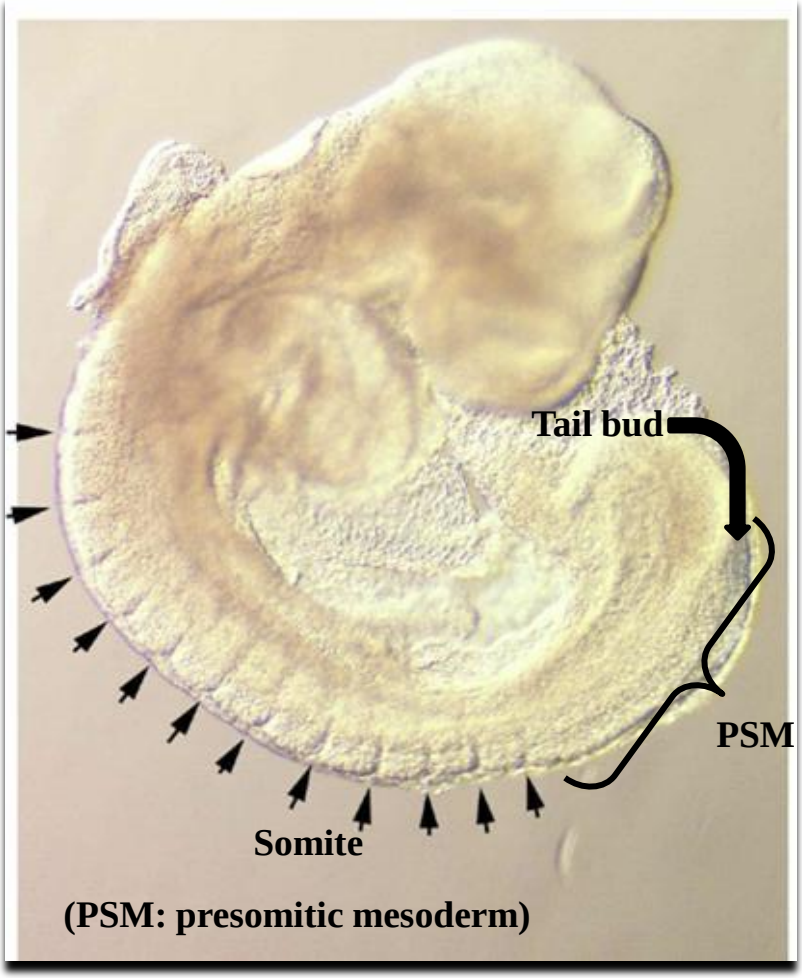


**Figure 1. Somitogenesis in mouse embryo at E9.0**

Somites, which are epithelialized blocks of cells, are periodically (every 2 hours) generated from the anterior end of presomitic mesoderm (PSM), while more cells is supplied by tail bud. Black arrows in picture indicate somites.

# Figure 2

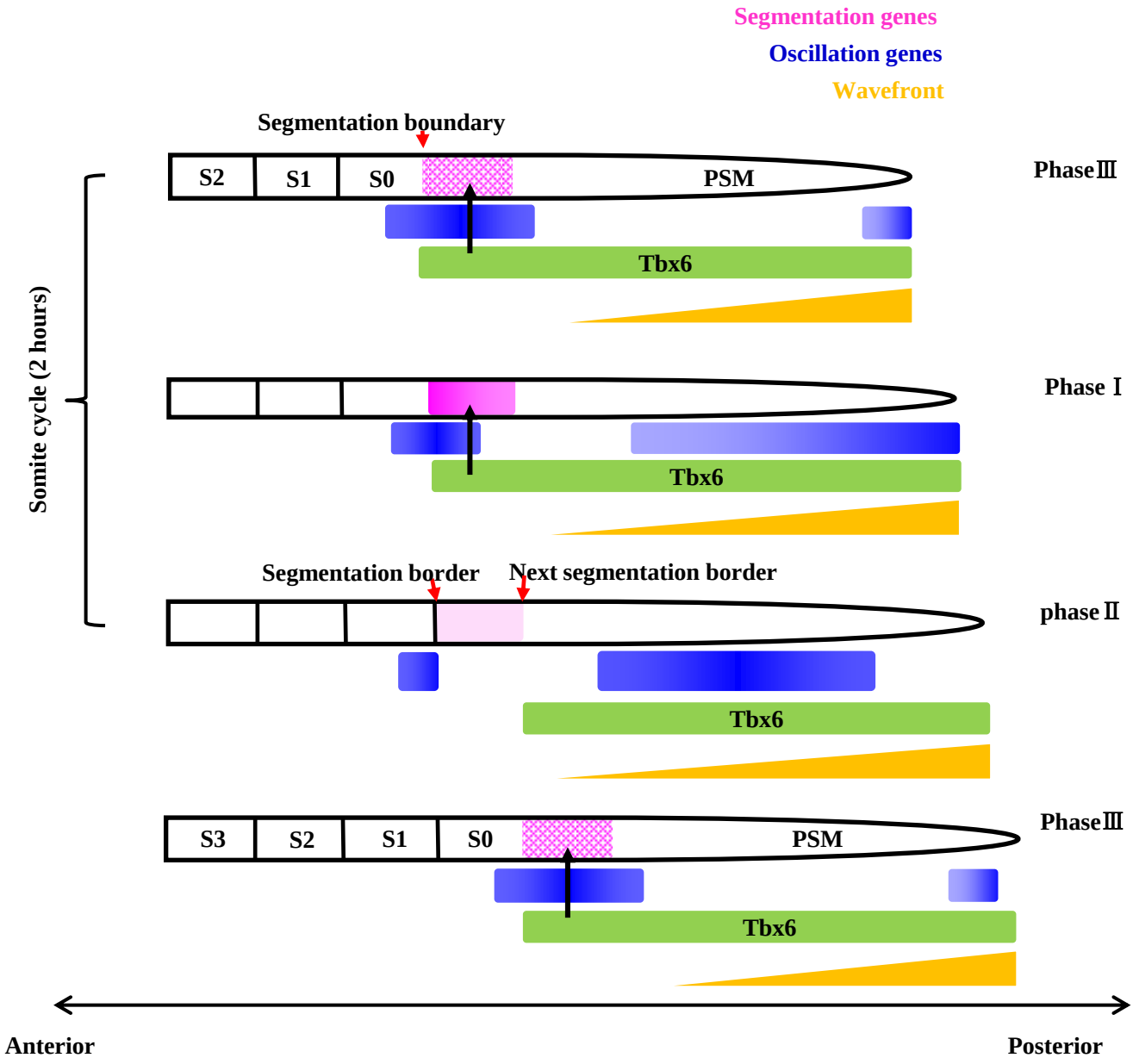


**Figure 2. 'clock and wavefront model' of somitogenesis**

The 'clock and wavefront model' explains somitogenesis as the interaction between two hypothetical elements. Oscillator synchronizes cells within the same dosal-ventral level into a same phase, whose activity like a wave move form posterior to anterior PSM, and establishes temporal periodicity in somitogenesis. While the regressing 'wavefront' is particular level which is characterized by a signaling threshold at which the cells become competent to respond to the segmentation clock signal. When the competent cells that pass through the wavefront receive the clock signal, they simultaneously activate *Mesp2*.

# Figure 3

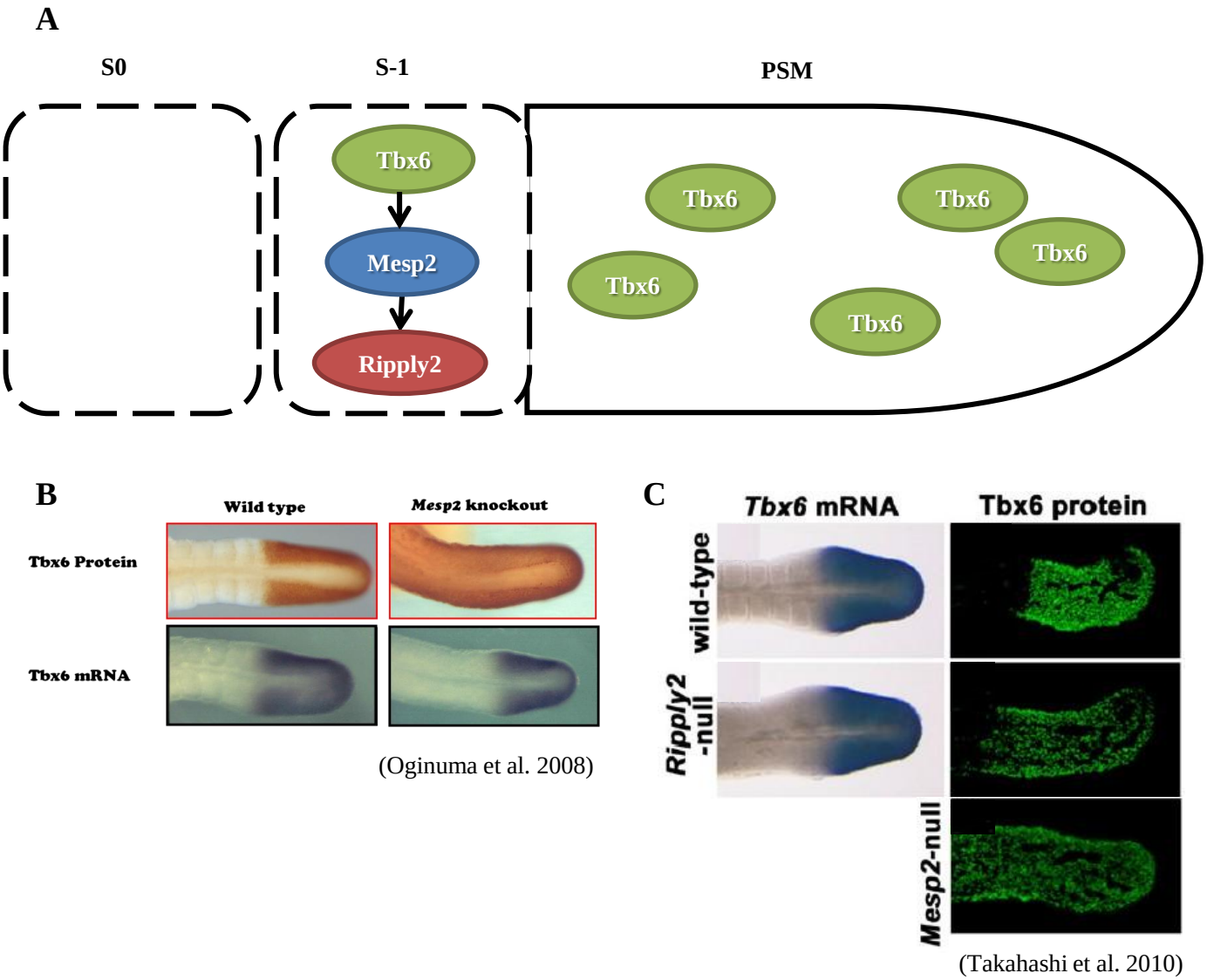


**Figure 3. The mechanism of periodic segmentation**

(A) Tbx6, a T-box family transcription factor expressed in PSM, induces the segmentation gene *Mesp2*. Mesp2 protein after translated in the anterior limit of its upstream factor Tbx6, Ripply2 triggers the degradation of Tbx6 by inducing another downstream factor-Ripply2. Here form a new Tbx6 anterior limit, which will become the next segmentation point.

(B) In *Mesp2*-null mice, Tbx6 protein expanded anteriorly, but the mRNA was not changed. Deficiency in *Ripply2* gene, Tbx6 protein but not mRNA expanded anteriorly, resembles *Mesp2*-null phenotype.

# Figure 4

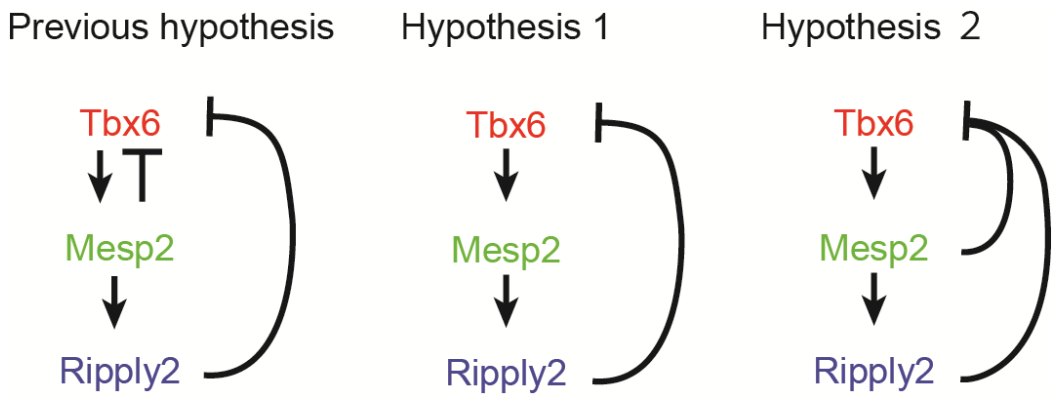


**Figure 4. Schematic representation of regulatory linkages in expected cascade of Tbx6, Mesp2 and Ripply2.**

Previous observations speculate that either Mesp2 or Ripply2 can lead to degradation of Tbx6, independent of each other. However, loss of *Ripply2* results in the prolonged expression of *Mesp2* but stabilizes Tbx6. This finding suggests that Mesp2 alone cannot induce Tbx6 degradation, indicating the possibility that Tbx6 suppression is a Mesp2-independent and Ripply2-required process (Hypothesis-1). Considering that both *Mesp2*-null and *Ripply2*-null embryos show Tbx6 domain expansion, both the factors might be essential but not sufficient for Tbx6 destabilization (Hypothesis-2).

# Figure 5

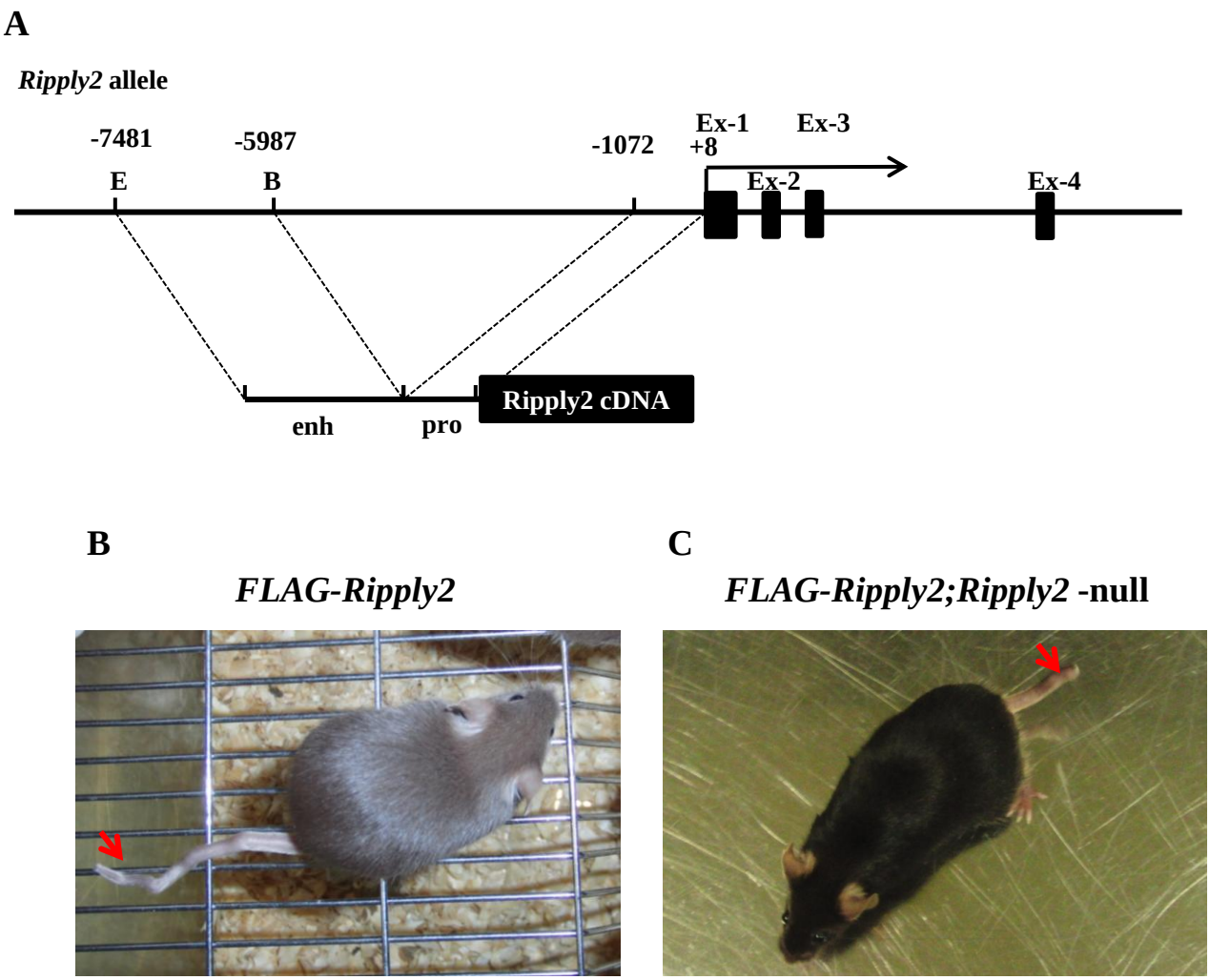


**Figure 5 Construct used for *FLAG-Ripply2* transgenic (TG) mice, and the morphology of resulting *FLAG-Ripply2* mice and *FLAG-Ripply2;Ripply2*-null mice.**

(A) The upper part of the figure shows the genomic organization of the *Ripply2* gene and the lower part shows the structure of the transgene. Two conserved regulatory regions were used to drive *Ripply2* expression in transgenic mice, a putative promoter adjacent to the initiator codon, and a putative enhancer at 6 kb upstream of transcription start site. (B) The *FLAG-Ripply2* TG mice showed phenotype indicating vertebra formation defects, such as shorter trunk, as well as shorter and kinked tail (red arrow). (C) *FLAG-Ripply2;Ripply2*-null mice survived but exhibited kinked tail resembling *FLAG-Ripply2* TG.

# Figure 6

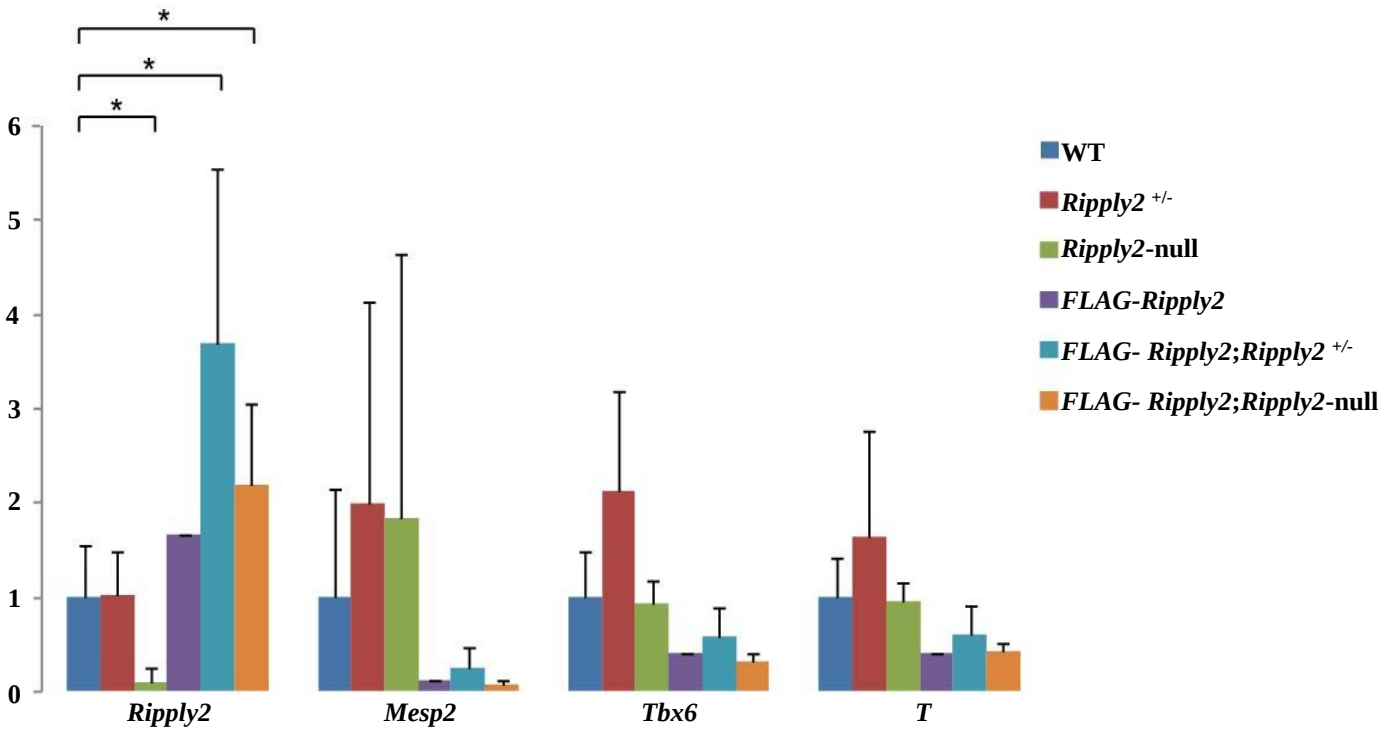


**Figure 6. Comparative analyses of expression levels of *Ripply2, Mesp2, Tbx6* and *T* transcript by RT-PCR.**

RNAs were prepared from single tail samples from WT (n=4), *Ripply2*$^{+/-}$ (n=6), *Ripply2*-null (n=3), *FLAG-Ripply2* (n=2), *FLAG-Ripply2;Ripply2*$^{+/-}$ (n=6), and *FLAG-Ripply2;Ripply2*-null (n=3) embryos. Samples were conducted RT-PCR analyses using primer set for *Ripply2*, *Mesp2*, *Tbx6* and *T*. The value of WT sample was set as 1. Data represent the mean+ s.d. $*P < 0.05$ in Brunner-Munzel Test.

# Figure 7

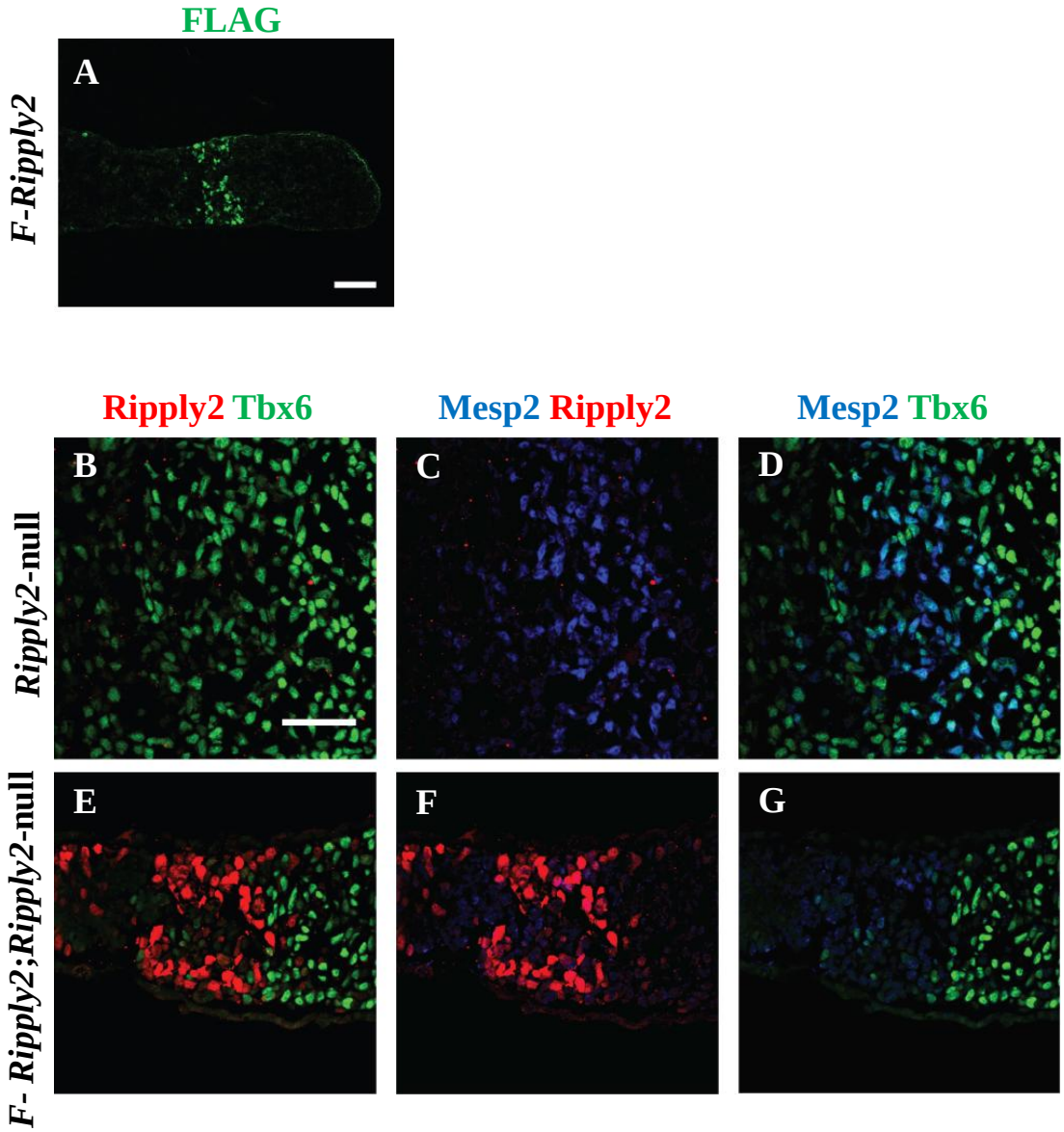


**Figure 7. Immunochemistry analysis for *FLAG-Ripply2*, *Ripply2*-null, and *FLAG-Ripply2;Ripply2*-null embryos.**

(A) FLAG-Ripply2 expression pattern detected by anti-FLAG antibody of *FLAG-Ripply2* TG embryo at E10.5. Scale bar: 100µm. (B-G) Expression patterns of Tbx6, Mesp2 and Ripply2 protein during somitogenesis were examined by immunostaining using antibodies against Tbx6, Mesp2, and Ripply2 with *Ripply2*-null (B, C, D) and *FLAG-Ripply2;Ripply2*-null TG embryos (E, F, G) at E10.5. Staining of the same slides were showed as Tbx6/Ripply2 (B, E), Mesp2/Ripply2 (C, F) and Tbx6/Mesp2 (D, G). Scale bar: 50µm.

# Figure 8

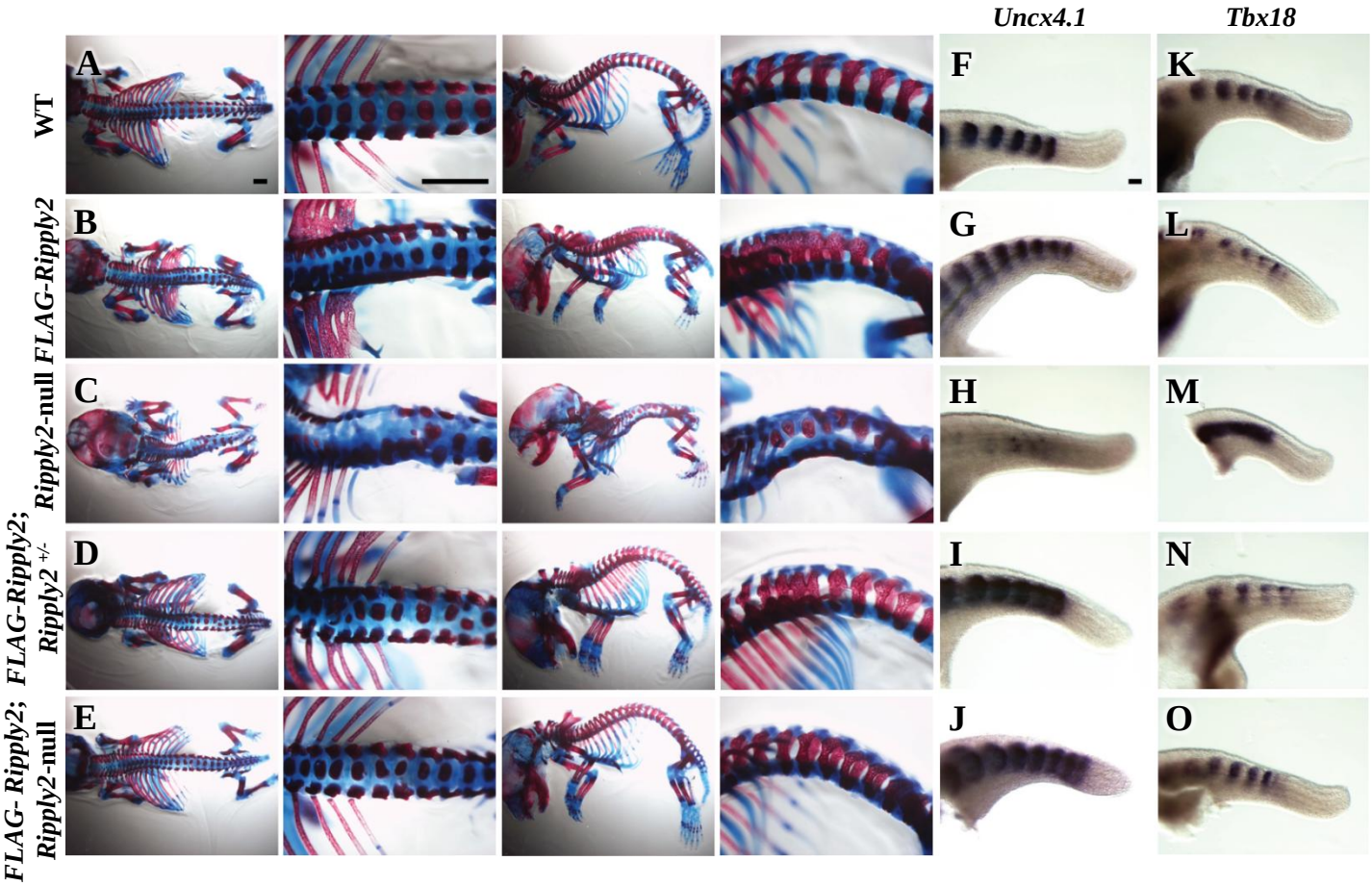


**Figure 8. The skeleton phenotype of *FLAG-Ripply2* TG mouse and associated gene expression**

Skeletal preparations and properties of somitic mesoderms were examined by staining with Alizarin Red-Alcian Blue at E18.5 (A-E) and by whole mount in situ hybridization using *Uncx4.1* (F-J) and *Tbx18* (K-O) probes. Genotypes of each sample are shown on the left. Dorsal and lateral views with higher magnifications are shown for skeletal samples. Wild type (WT) mice showed vertebra and ribs with regular shape (A) and a normal segmental pattern in both *Uncx4.1* (F) and *Tbx18* (K). There was minor defect in vertebra and ribs in *FLAG-Ripply2* embryos (B). *Ripply2*-null fetus showed rostralized phenotype, including fewer pedicles or neural arches (C) and expanded *Tbx18* expression (M). *FLAG-Ripply2;Ripply2*$^{+/-}$ showed phenotype similar to *FLAG-Ripply2* (D). *FLAG-Ripply2;Ripply2*-null phenotype (E) and the gene expression patterns (J, O) are well rescued compared with *Ripply2*-null fetus. Scale bars: 1mm for skeletal pictures. 100µm for samples stained for in situ hybridization.

# Figure 9

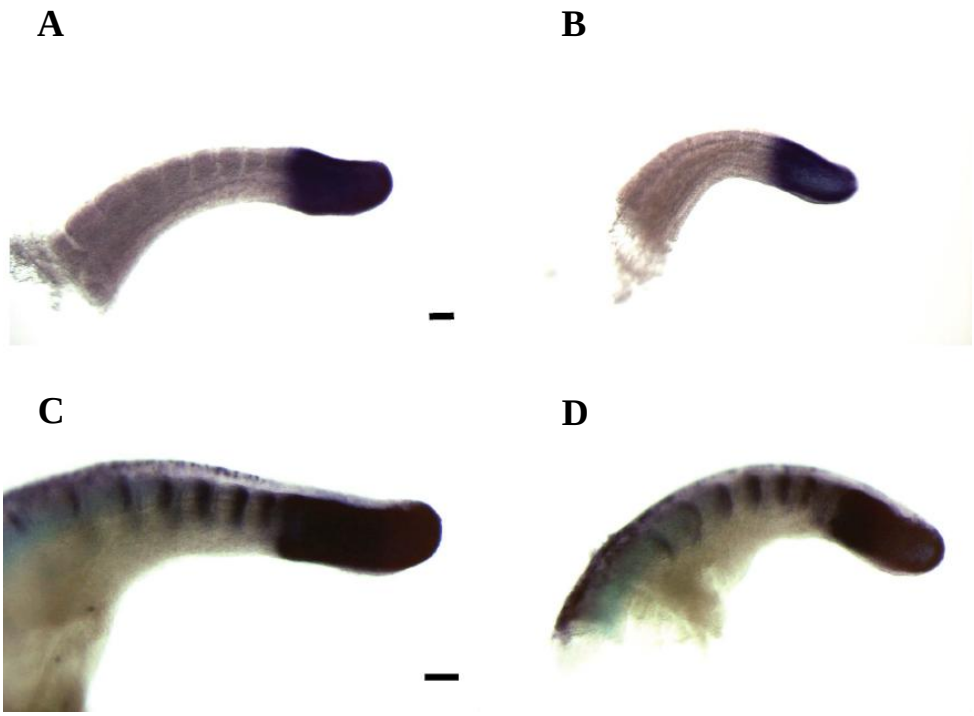


**Figure 9. Expression pattern of *Tbx6* and *Dll1* was unchanged in WT and *FLAG-Ripply2* embryos.**

Whole mount in situ hybridization for *Tbx6* mRNA (A-B) and *Dll1* mRNA (C-D) in WT (A, C) and *FLAG-Ripply2* (B, D) embryos. Scale bars: 100µm.

# Figure 10

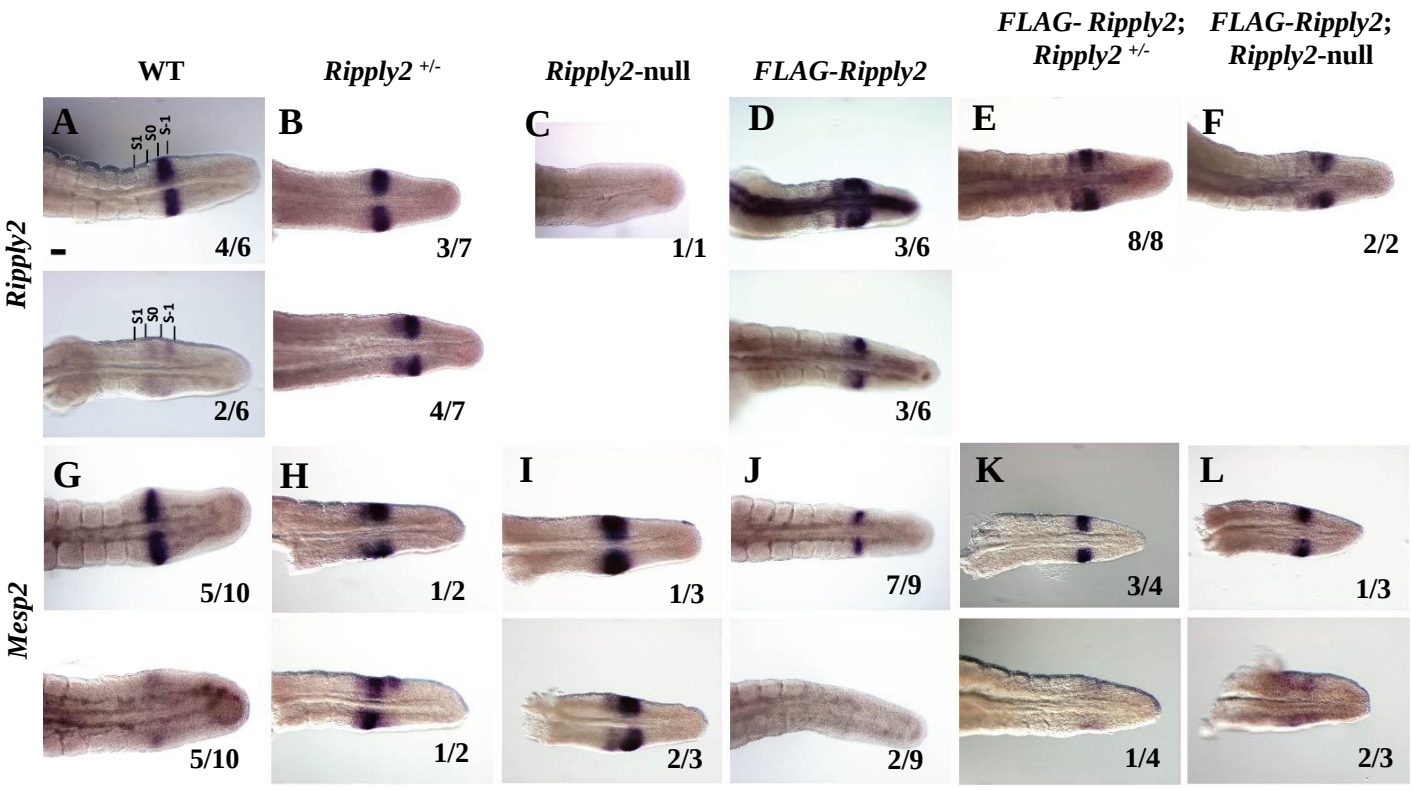


**Figure 10. Gene expression analyses in *FLAG-Ripply2* TG embryos**

Whole-mount in situ hybridization was conducted to characterize somitogenesis. Different patterns of mRNA expression of *Ripply2* (A-F), *Mesp2* (G-L) in WT (A,G), *Ripply2*$^{+/-}$ (B,H), *Ripply2*-null (C,I), *FLAG-Ripply2* (D,J), *FLAG-Ripply2;Ripply2*$^{+/-}$ (E,K) and *FLAG-Ripply2;Ripply2*-null (F,L) were shown. *Ripply2* in *FLAG-Ripply2* embryos (D) was much stronger than WT (A) and *Ripply2*$^{+/-}$ (B) and showed several strips. The *Ripply2* expression in *FLAG-Ripply2;Ripply2*$^{+/-}$ (E) and *FLAG-Ripply2;Ripply2*-null (F) were also clearly up-regulated. *Mesp2* expression was expanded in *Ripply2*$^{+/-}$ (H) and *Ripply2*-null (I) compared with WT (G), while it was down-regulated in FLAG-Ripply2 (J), but it was recovered in *FLAG-Ripply2;Ripply2*$^{+/-}$ (K) and FLAG-Ripply2;*Ripply2*-null (L). Scale bar: 100µm.

# Figure 11

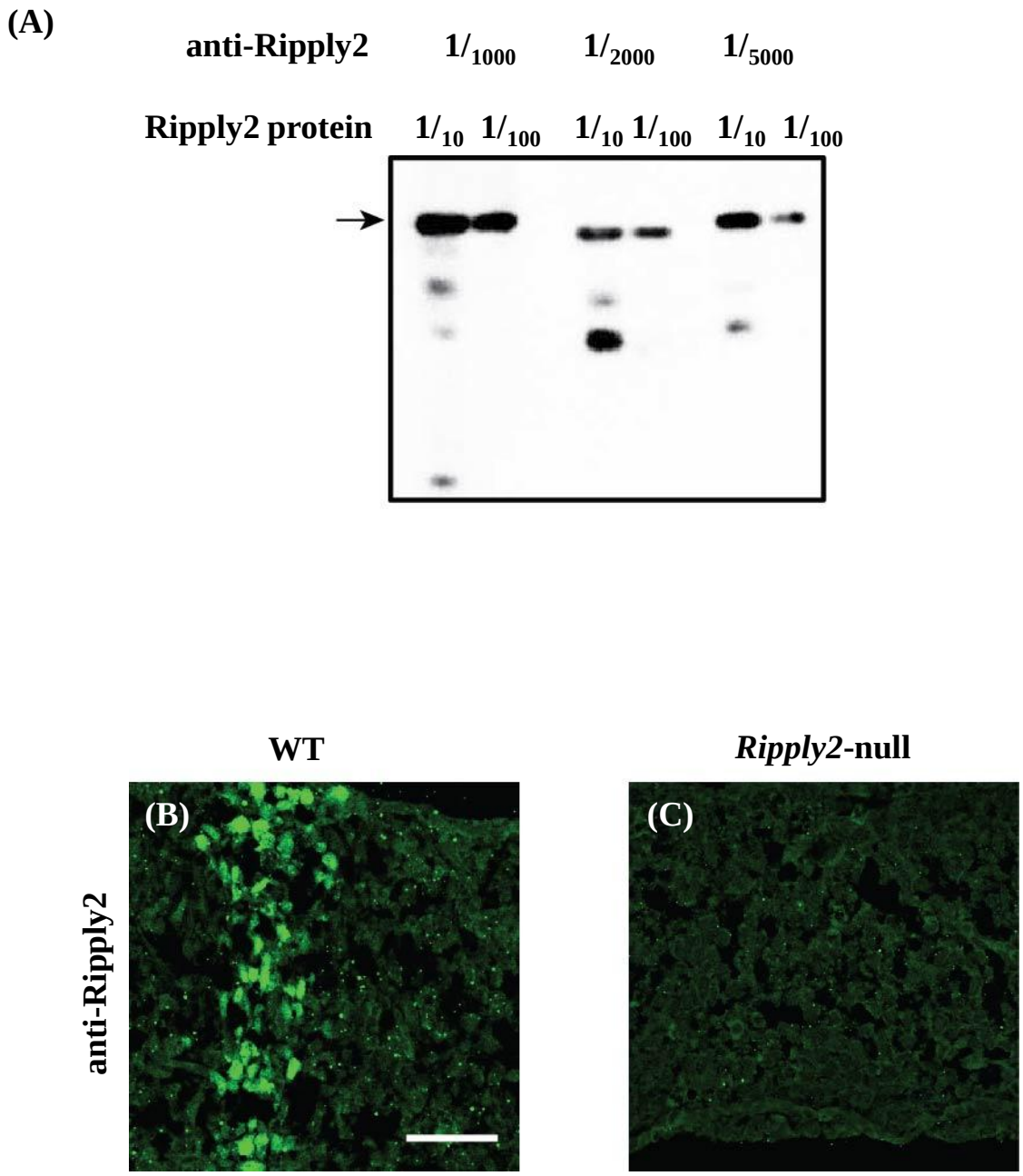


**Figure 11. Specificity of anti-Ripply2 antibody produced and used in this study.**

(A) Affinity purified antibody was diluted 1/1000, 1/2000 and 1/5000 and western blotting analyses were conducted using antigen purified from bacterially expressed Ripply2 protein. Arrow indicates Ripply2 band. (B-C) The anti-Ripply2 antibody detected endogenous Ripply2 expression in WT embryo (B) but not in *Ripply2*-null embryos (C). Scale bar, 50μm.

# Figure 12 (A)

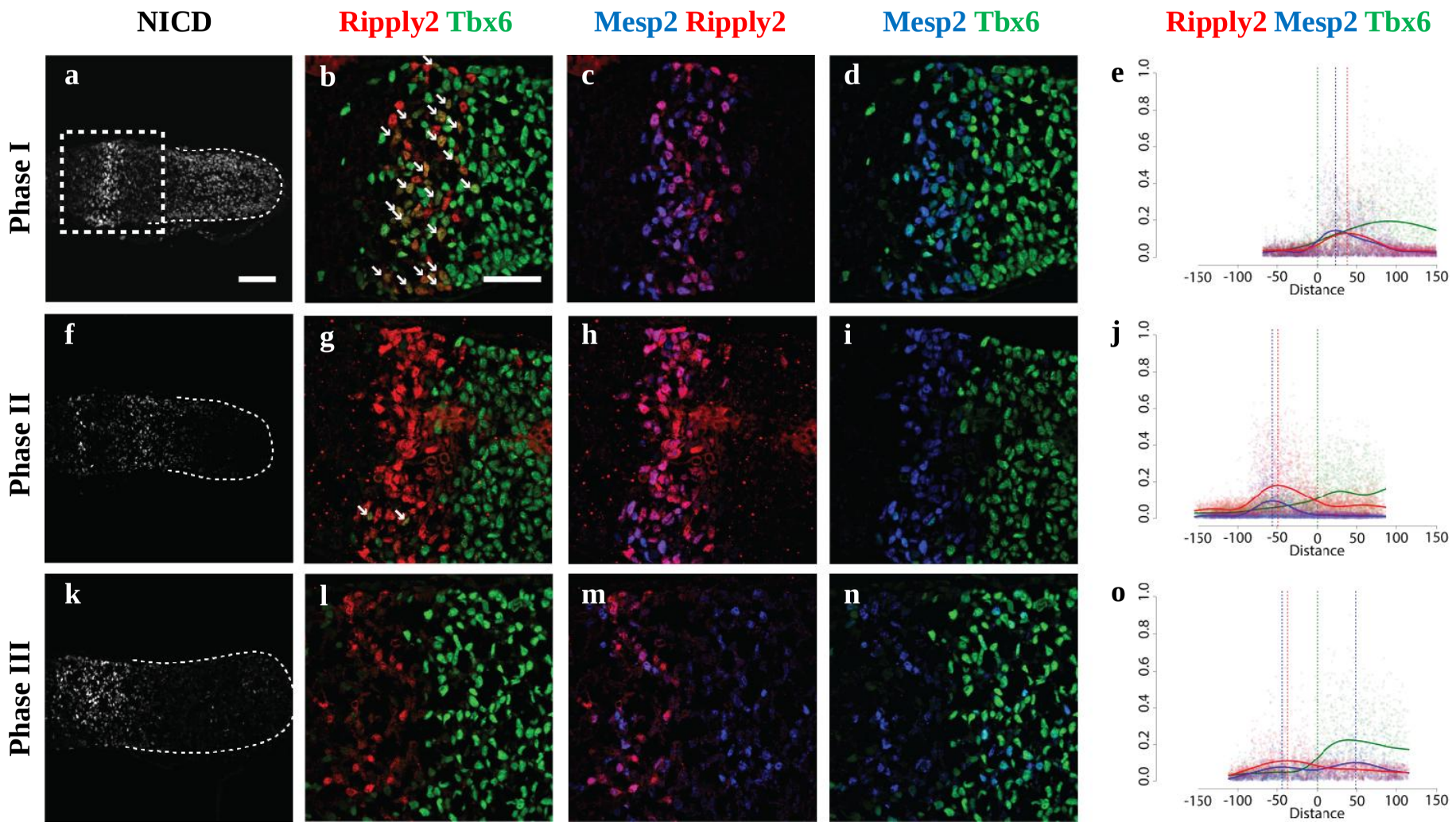
NICD
Ripply2 Tbx6
Mesp2 Ripply2
Mesp2 Tbx6
Ripply2 Mesp2 Tbx6
Phase I
Phase II
Phase III
a
b
c
d
e
f
g
h
i
j
k
l
m
n
o
0.0
0.2
0.4
0.6
0.8
1.0
-150
-100
-50
0
50
100
150
Distance

**(B)**

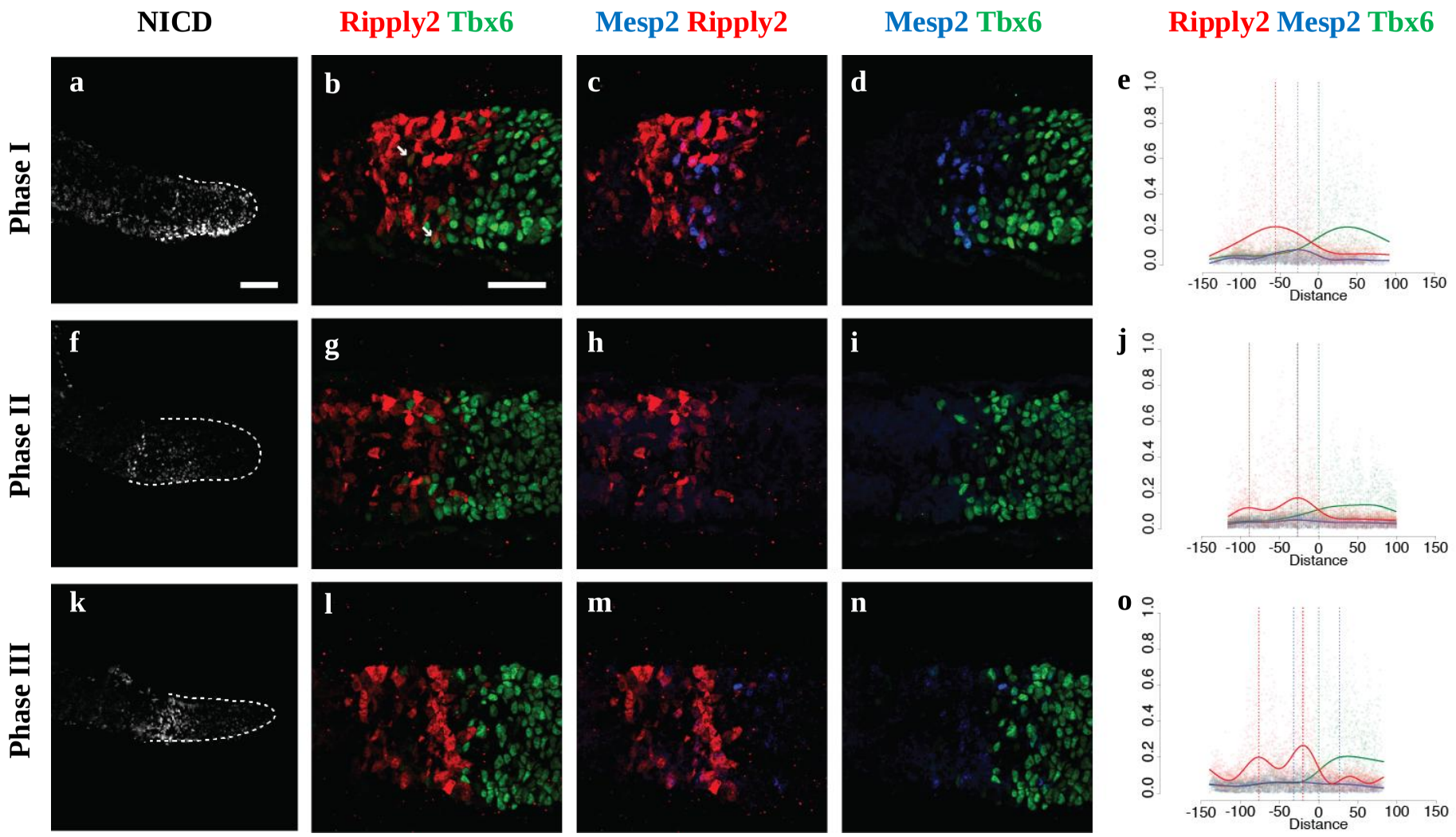
NICD
Ripply2 Tbx6
Mesp2 Ripply2
Mesp2 Tbx6
Ripply2 Mesp2 Tbx6
Phase I
Phase II
Phase III
a
b
c
d
e
f
g
h
i
j
k
l
m
n
o
0.0 0.2 0.4 0.6 0.8 1.0
-150 -100 -50 0 50 100 150
Distance

# (C)

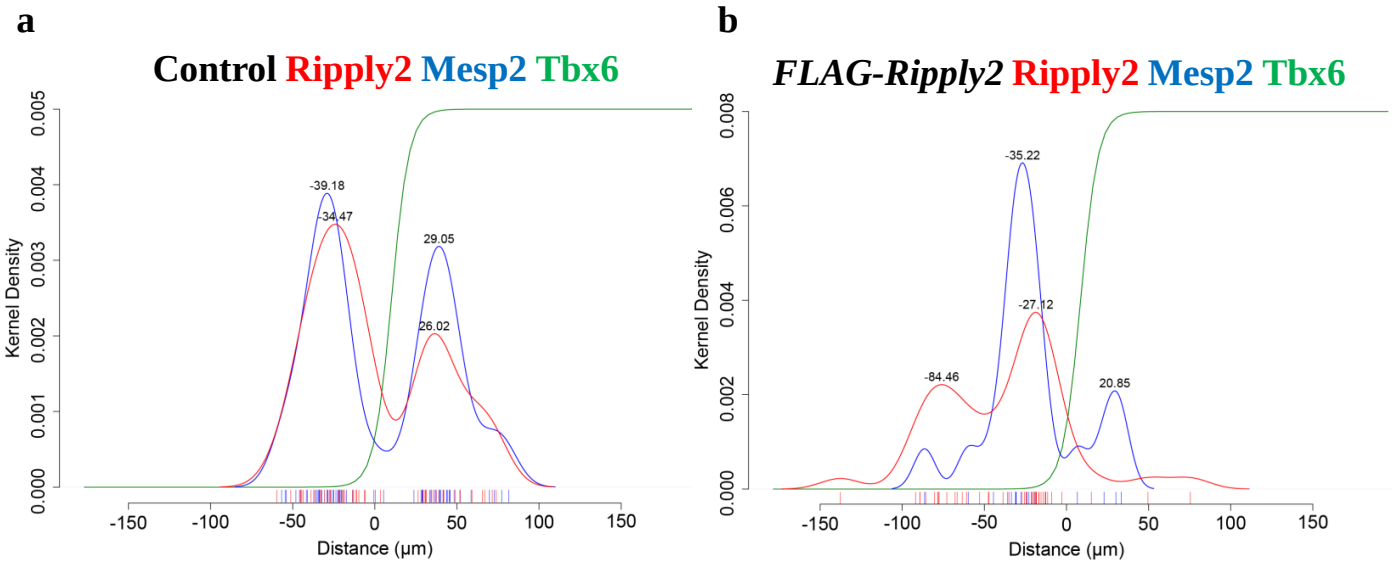


**Figure 12. Periodical expression changes of Tbx6, Mesp2 and Ripply2 proteins in control and *FLAG-Ripply2* TG embryos**

Spatio-temporal patterns of active Notch signal (NICD), Tbx6, Mesp2 and Ripply2 protein during somitogenesis were examined by immunostaining using antibodies against NICD, Tbx6, Mesp2, and Ripply2 with control (A) and *FLAG-Ripply2* TG embryos (B) at E10.5. Embryos at three individual time points during a segmentation cycle were arranged: phase I (a-e), phase II (f-j) and phase III (k-o). Three phases were judged by the localization of oscillating Notch activity in the serial section of same embryo used for following triple staining (a, f, k). Scale bar: 100μm. Triple immunostaining patterns obtained from single slides were shown as Ripply2/Tbx6 (b,g,l), Ripply2/Mesp2 (c, h, m), and Mesp2/Tbx6 (d, i, n), respectively. White arrows indicate overlapped signals of Tbx6 and Ripply2. Scale bar: 50μm. These pictures were analyzed by grid-based methods and the results were shown as scatter plots of Tbx6 (green), Mesp2 (blue) and Ripply2 (red) fluorescent intensities (Y-axis in arbitrary unit) to distance from Tbx6 expression anterior limit (X-axis in μm) are shown in (A e, j, o) and (B e, j, o). Positive or negative value of the distance indicates a plot locating caudal (posterior) or rostoral (anterior) side of the limit respectively. Solid lines are the intensities' spline smoothing regression to the distance. A summit of the spline curve is regarded as a representative of location of the stripe and an inflection point of the Tbx6 spline curve is used for a calibration of the actual Tbx6 anterior limit. Colored dotted lines are either the anterior limit of Tbx6 (green) or the locations of Mesp2 (blue) and Ripply2 (red) stripes.

(C) Locations of Mesp2 (blue) and Ripply2 (red) stripes are accumulated then used for estimation of stripe's location by kernel density estimation. Tags on the X-axis indicate observed locations of the stripes. For pattern-by-pattern representations, see SFig. 7. Tbx6 anterior limits were calibrated as Distance = 0. (a) In control, Mesp2 and Ripply2 show 2 main locations on both sides of the limit. Number of image-sets analyzed is 49 (b) In *FLAG-Ripply2* TG, estimated location of Mesp2 stripes are very similar to that of control, while Ripply2 shows ectopic stripes at further anterior region (at -84.46 μm). Number of image-sets analyzed is 21.

# Figure 13

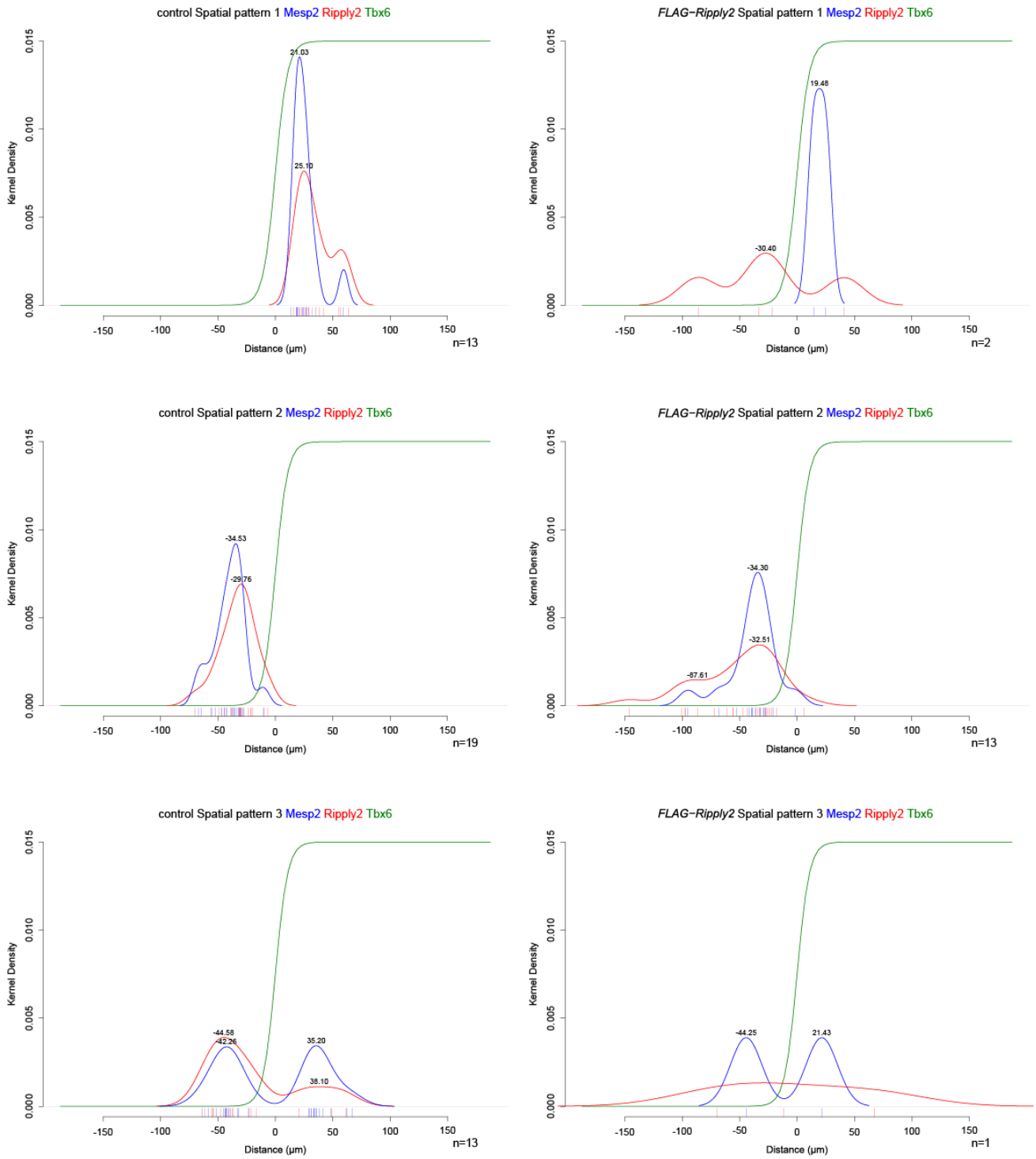


**Figure 13. Pattern-by-pattern representations of Figure 3C.**

Locations of Mesp2 and Ripply2 stripes were estimated by kernel density estimation applied onto dataset from each spatial pattern. Relativities of Mesp2 stripe to Tbx6 limit (Distance = 0) clearly show the 3 patterns in control. Locations of Mesp2 stripe at pattern 2 are identical between control and *FLAG-Ripply2* TG. Wilcoxon rank sum test supports the notion. In the case of control, Ripply2 stripes well correspond with Mesp2 stripes in all three patterns, while aberrant and ectopic Ripply2 stripes are obvious in *FLAG-Ripply2* TG.

# Figure 14

**A**

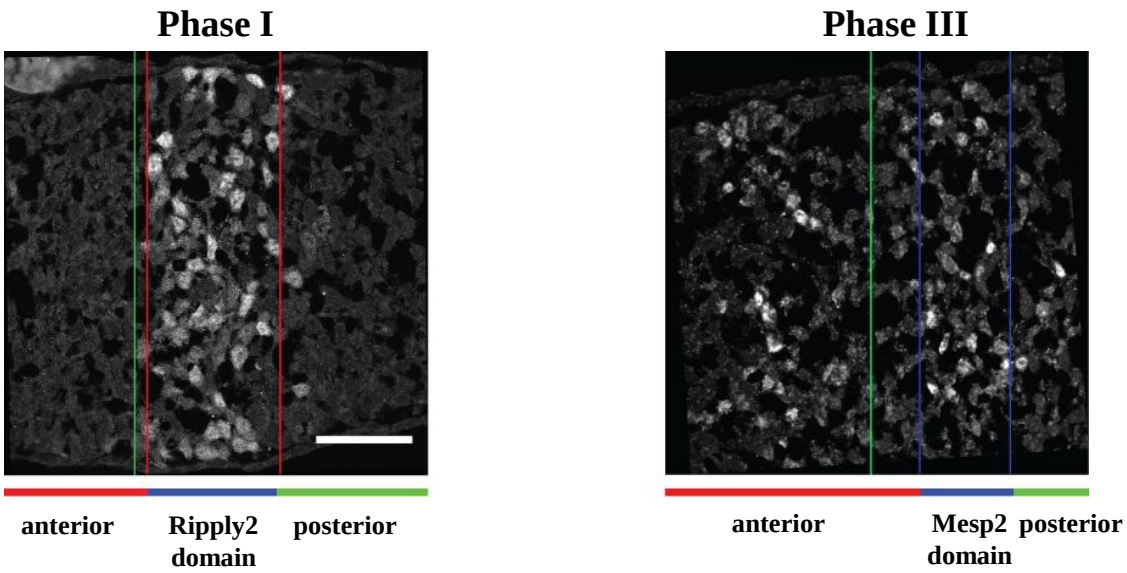


**B**

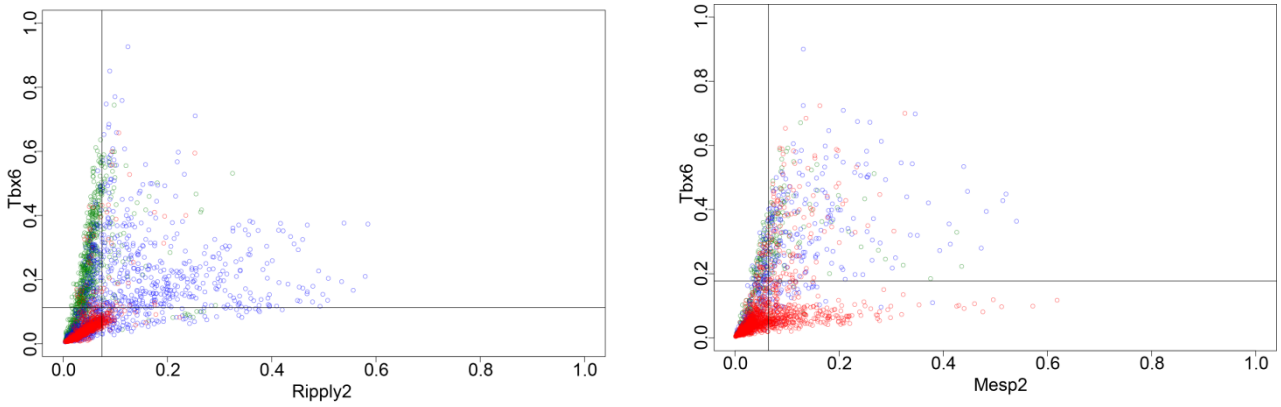


**C**

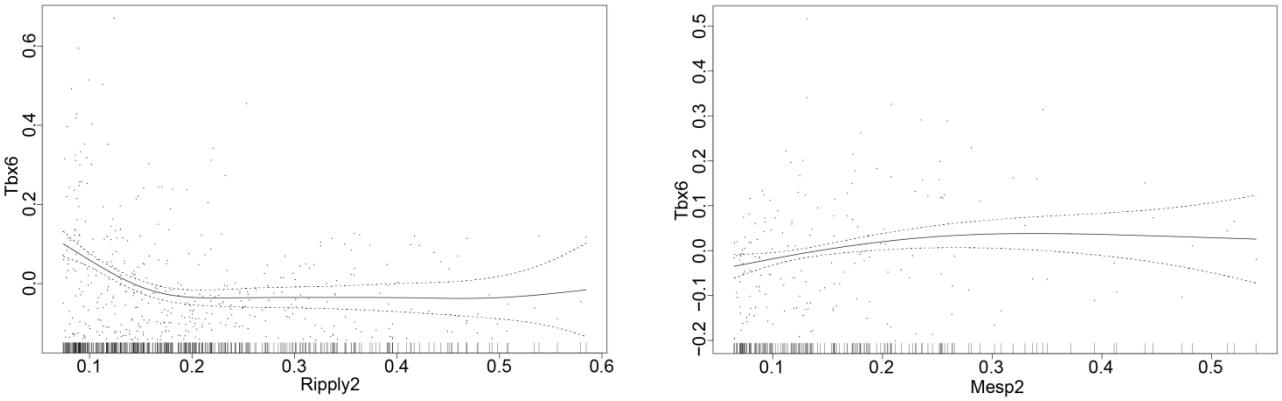

**Figure 14. Non-linear regression analysis between Tbx6 and Ripply2/Mesp2**

(A) shows anterior domain, Ripply2 (left) or Mesp2 (right) expression domain in S-1, and posterior domain in control embryos of phase I and phase III used in Fig. 3A. Lines under the picture indicated the domains used in Scatter plot. Red bar, anterior domain; blue bar, Ripply2, or Mesp2 domain; green bar, posterior domain. Scale bar: 50μm. Width of the expression stripe is defined by inflection points of either Ripply2 (red lines) or Mesp2 (blue lines) spline curve (Fig. 3A e, o). Tbx6 expression front is shown by green line. (B) Scatter plots of 3 regions (anterior in red, stripe domain in blue and posterior in green) defined by the stripe. Generally, Tbx6 intensity is high in the posterior (green) and low in the anterior (red). Median intensities of Tbx6 (0.113 in phase I, 0.177 in phase III), Ripply2 (0.074) and Mesp2 (0.064) in the stripe domain are used as thresholds of the expression level (solid lines). Subset of the data by the thresholds is further processed using a regression analysis. (C) Non-linear (spline smoothing) regression between Tbx6 and either Ripply2 or Mesp2 shows a difference of the Tbx6 response to the Ripply2/Mesp2. A strong negative correlation is observed at less than 0.2 of Ripply2 intensity, while almost nil correlation at more than the 0.2. In the case of Mesp2, a weak positive correlation is observed regardless of Mesp2 intensity.

# Figure 15

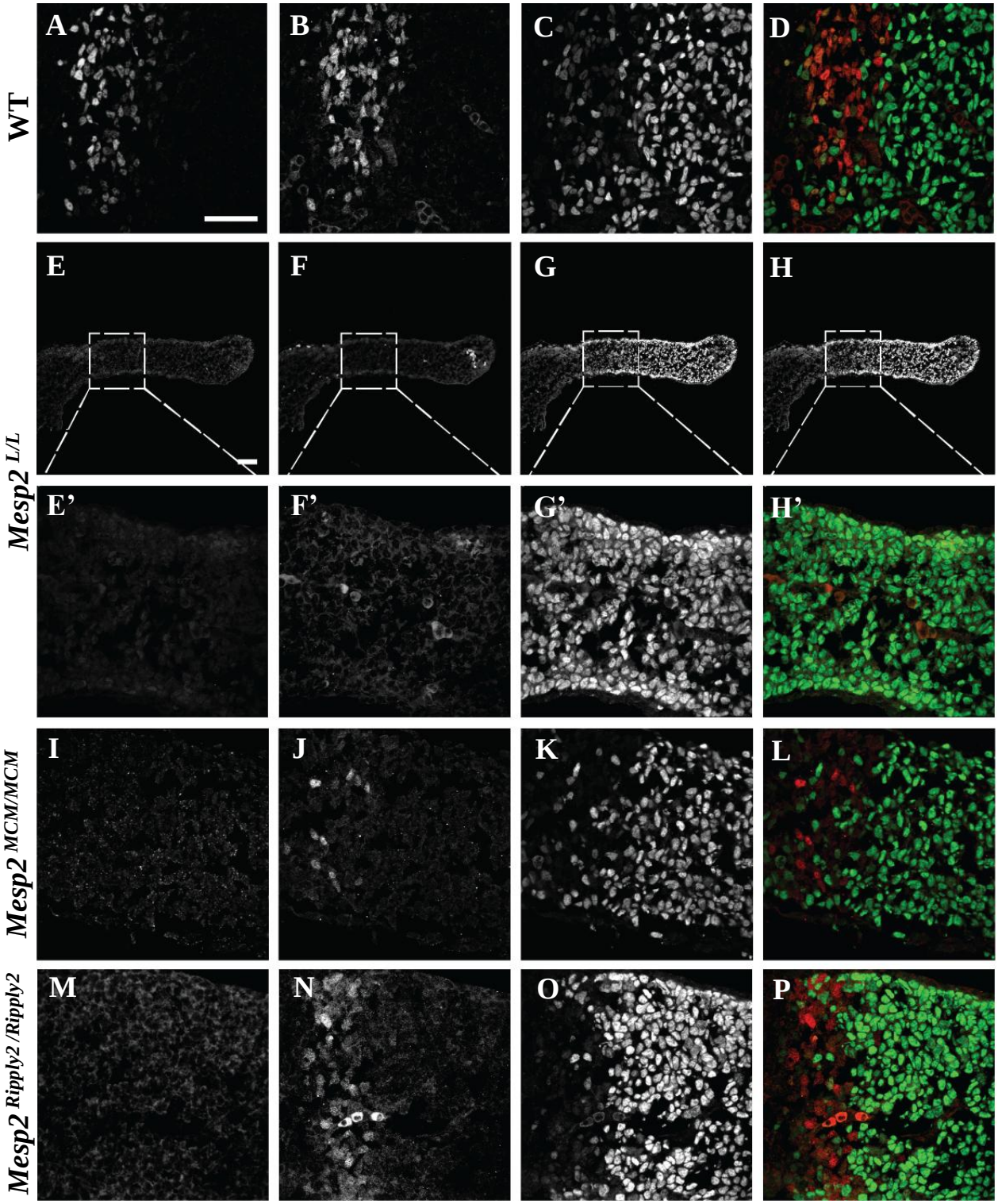


**Figure 15. Expression changes of Tbx6, Mesp2 and Ripply2 proteins in *Mesp2*-null mutant and *Mesp2*$^{Ripply2/Ripply2}$ embryos**

Tbx6, Mesp2 and Ripply2 proteins were examined by immunostaining using antibodies against Tbx6, Mesp2, and Ripply2 in WT (A-D), *Mesp2*$^{L/L}$ (E-H, E'-H'), *Mesp2*$^{MCM/MCM}$ embryos (I-L) and *Mesp2*$^{Ripply2/Ripply2}$ (M-P) at E10.5. (E'-H') Magnified images corresponding region indicated in (E-H) are shown. Scale bars: 100 µm for E-H, 50 µm for others.

# Figure 16

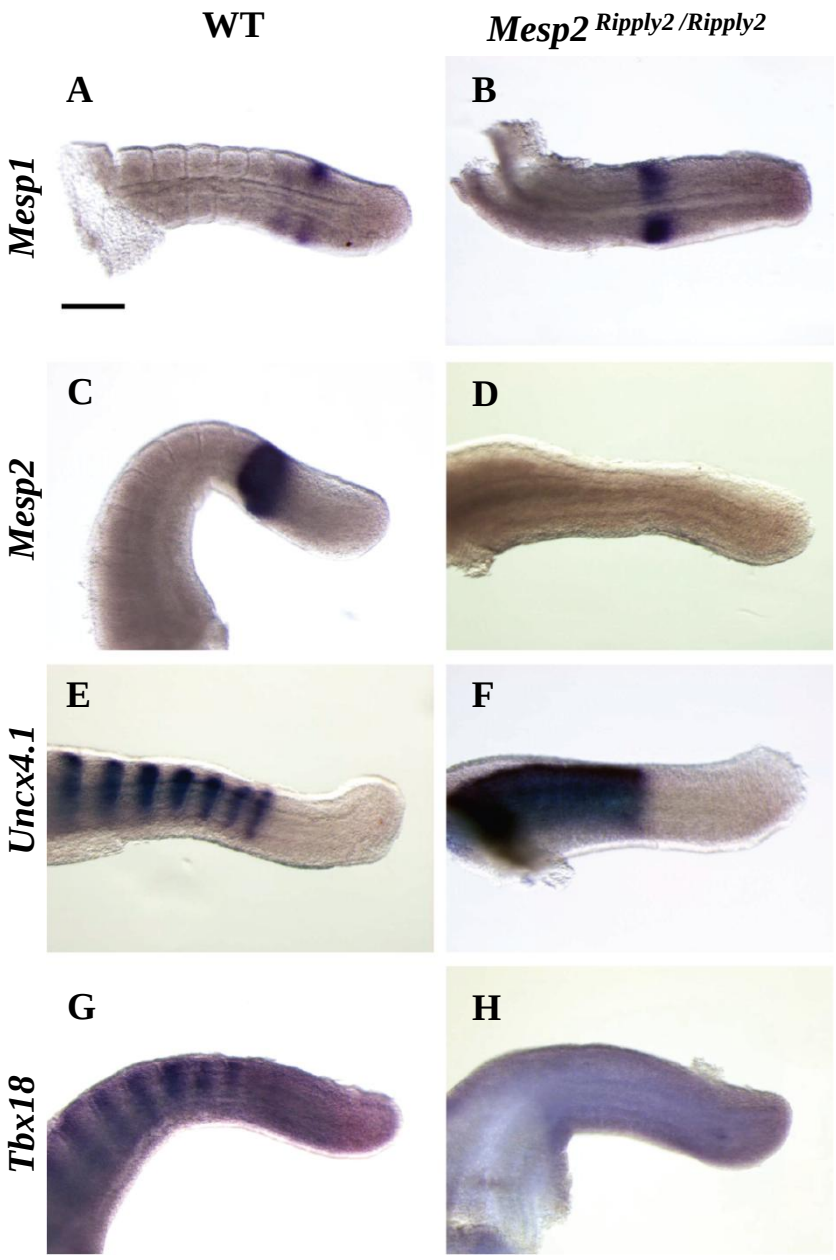


**Figure 16. *Mesp2*$^{Ripply2/Ripply2}$ exhibited caudalized phenotype.**

Whole mount in situ hybridization for *Uncx4.1* (A-B) and *Tbx18* mRNA (C-D) in WT (A, C) and *Mesp2*$^{Ripply2/Ripply2}$ (B, D) embryos. Scale bars: 200µm.

# Figure 17

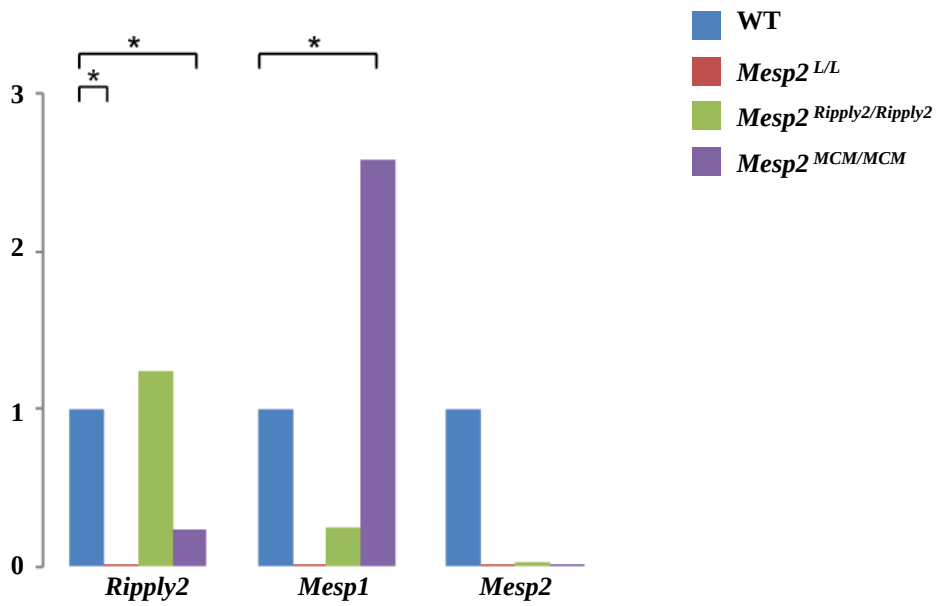


**Figure 17. RT-PCR result for WT, *Mesp2*$^{L/L}$ , *Mesp2*$^{Ripply2/Ripply2}$ and *Mesp2*$^{MCM/MCM}$ embryos**

RNAs were prepared from single tail samples from WT (n=3), *Mesp2*$^{L/L}$ (n=7), *Mesp2*$^{Ripply2/Ripply2}$ (n=6) and *Mesp2*$^{MCM/MCM}$ (n=1) embryos. * $P$ <0.05 in Brunner-Munzel Test.

# Figure 18

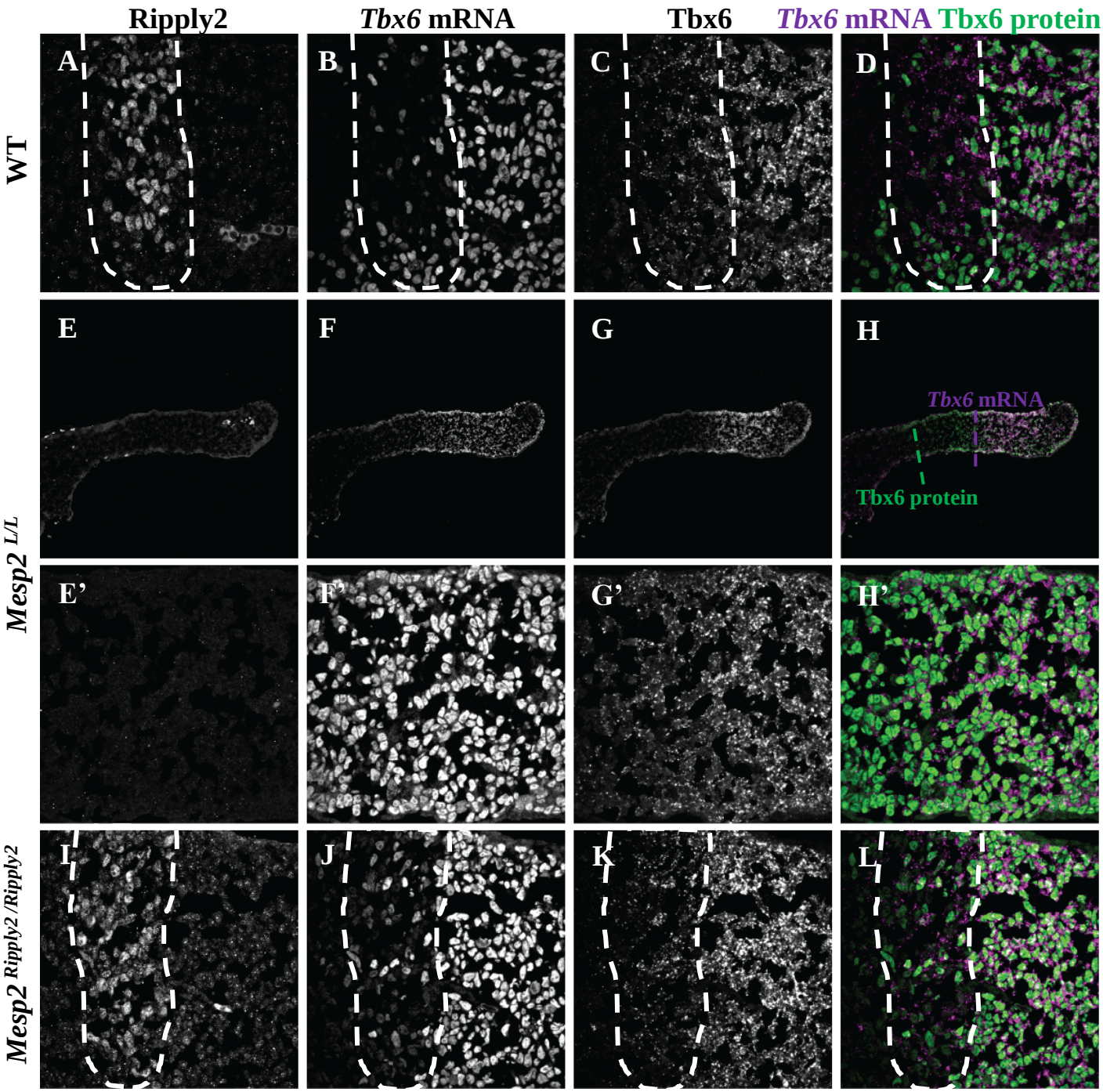


**Figure 18. Anterior limit of *Tbx6* mRNA did not changed in *Mesp2* $^{L/L}$ or *Mesp2* $^{Ripply2/Ripply2}$ embryos.**

Figures showed in situ hybridization of *Tbx6* mRNA (B, F, F', J) and immunostaining of Ripply2 (A, E, E', I) and Tbx6 (C, G, G', K) in control (A-D), *Mesp2*$^{L/L}$ (E-H, E'-H') and *Mesp2*$^{Ripply2/Ripply2}$ (I-L) samples. (D, H, H', L) showed merged pictures. Scale bar: 50µm.

# Figure 19

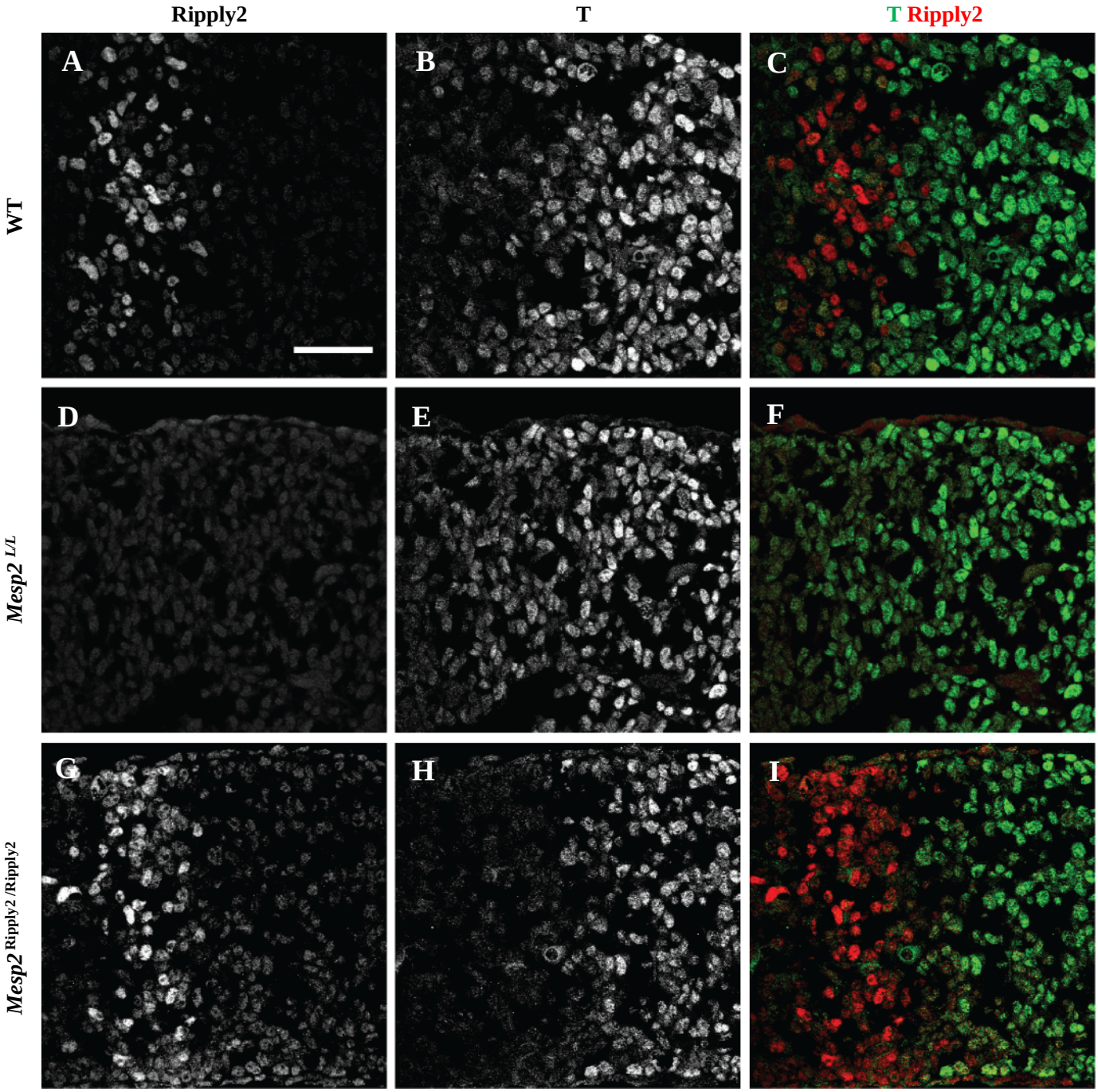


**Figure 19. Anterior limit of T protein could be altered by Ripply2.**

Figures showed immunostaining of Ripply2 (A, D, G) and T (B, E, H) in control (A-C), *Mesp2*$^{L/L}$ (D-F) and *Mesp2*$^{Ripply2/Ripply2}$ (G-I) samples. (C, F, I) showed merged pictures. Scale bar: 50µm.

# Figure 20

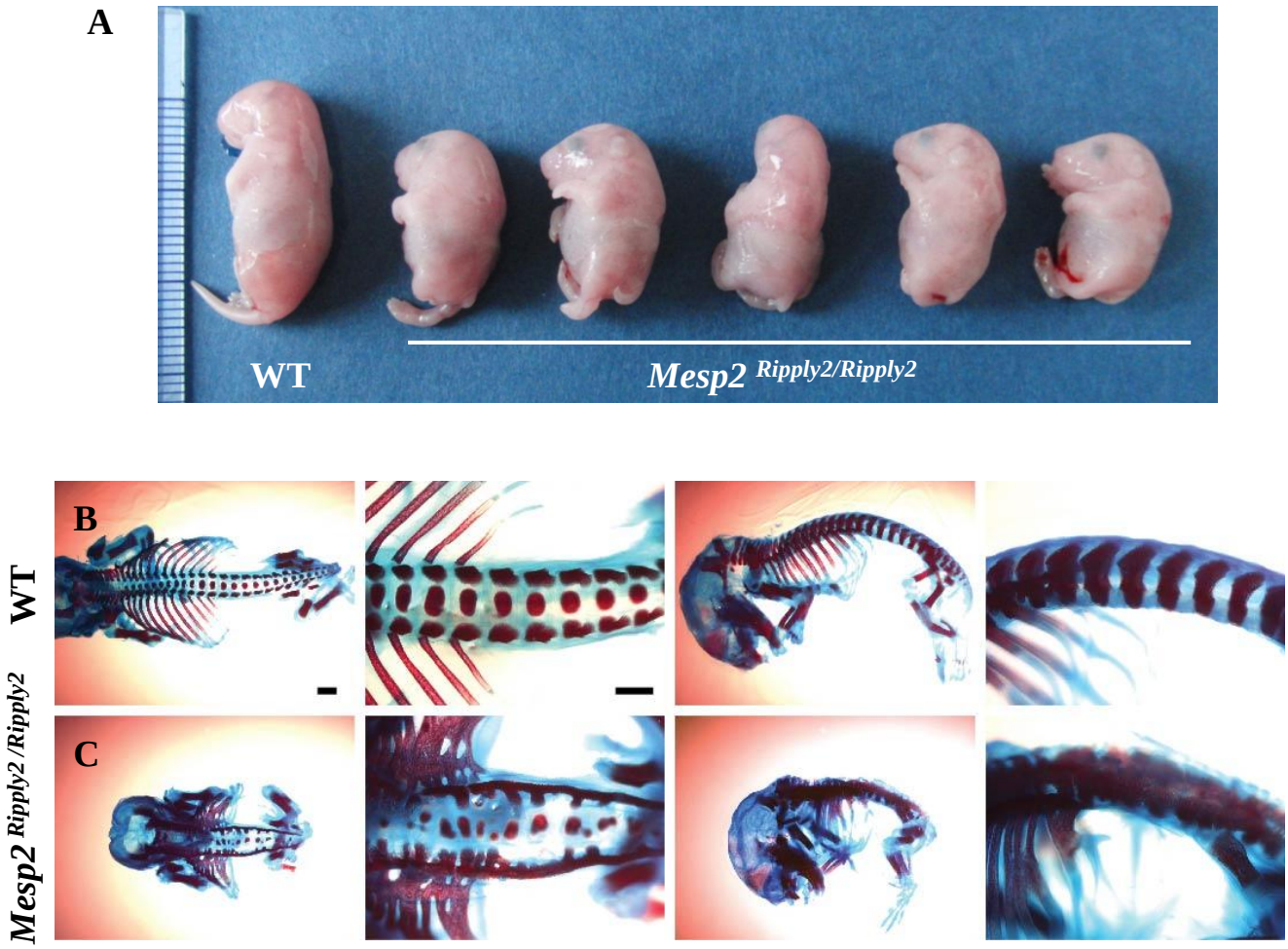


**Figure 20 *Mesp2 Ripply2/Ripply2* exhibited deficiency in somitogenesis**

(A) *Mesp2 Ripply2/Ripply2* of E18.5 showed truncated trunk and tail. (B-C) Skeletal samples of WT (A) and *Mesp2 Ripply2/Ripply2* mouse at E18.5 were stained with Alizarin Red-Alcian Blue.

# Figure 21

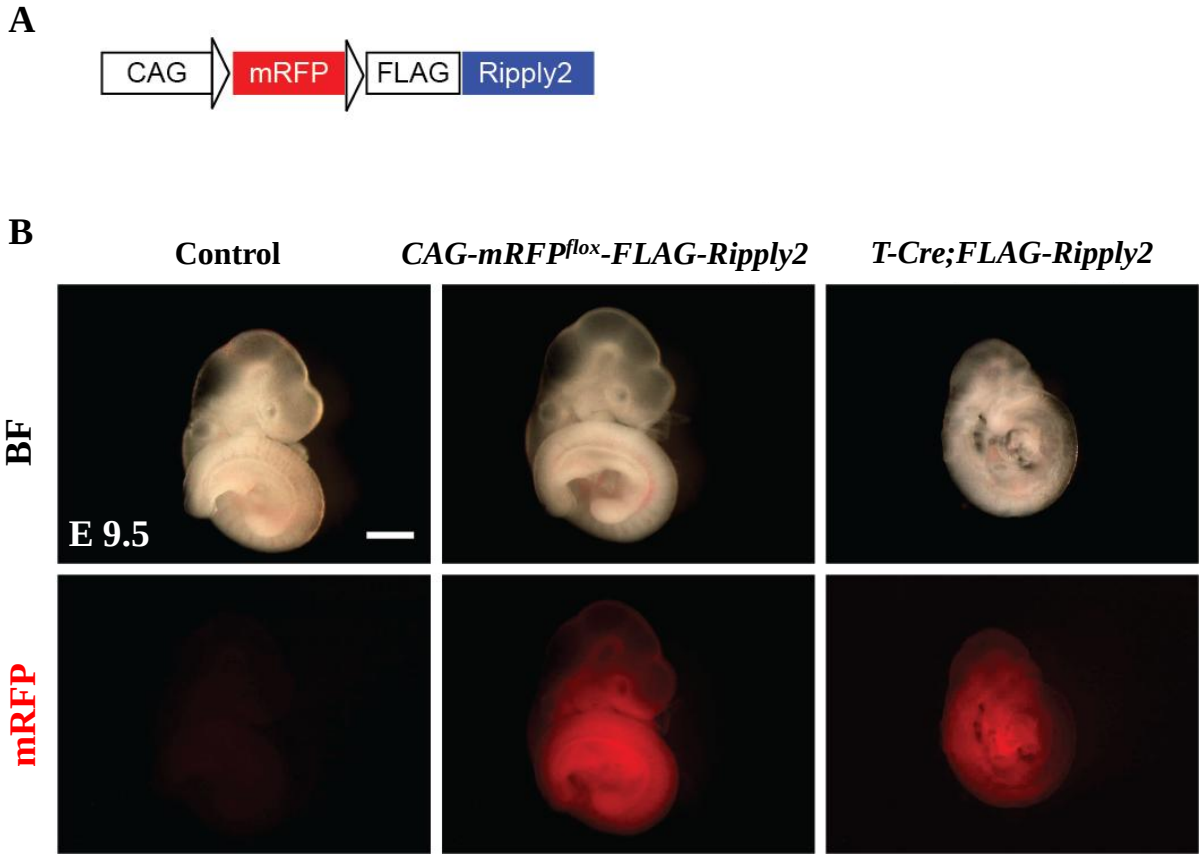


**Figure 21. Strategy used for conditional ectopic Ripply2-expressing mouse and the resulting TG mouse**

(A) Transgene construct used for ectopic Ripply2 expression. *CAG* promoter was attached to a *FLAG* modified *Ripply2* cDNA with a floxed *mRFP* between them. (B) mRFP expression pattern was shown to monitor Cre recombinase activity. There is no mRFP expression in the wild-type embryo (left). Without Cre recombinase, mRFP is expressed over the entire body of transgenic embryo (center). After crossing with *T-Cre*, mRFP expression is reduced at posterior embryo (right). Scale bar: 400μm.

# Figure 22

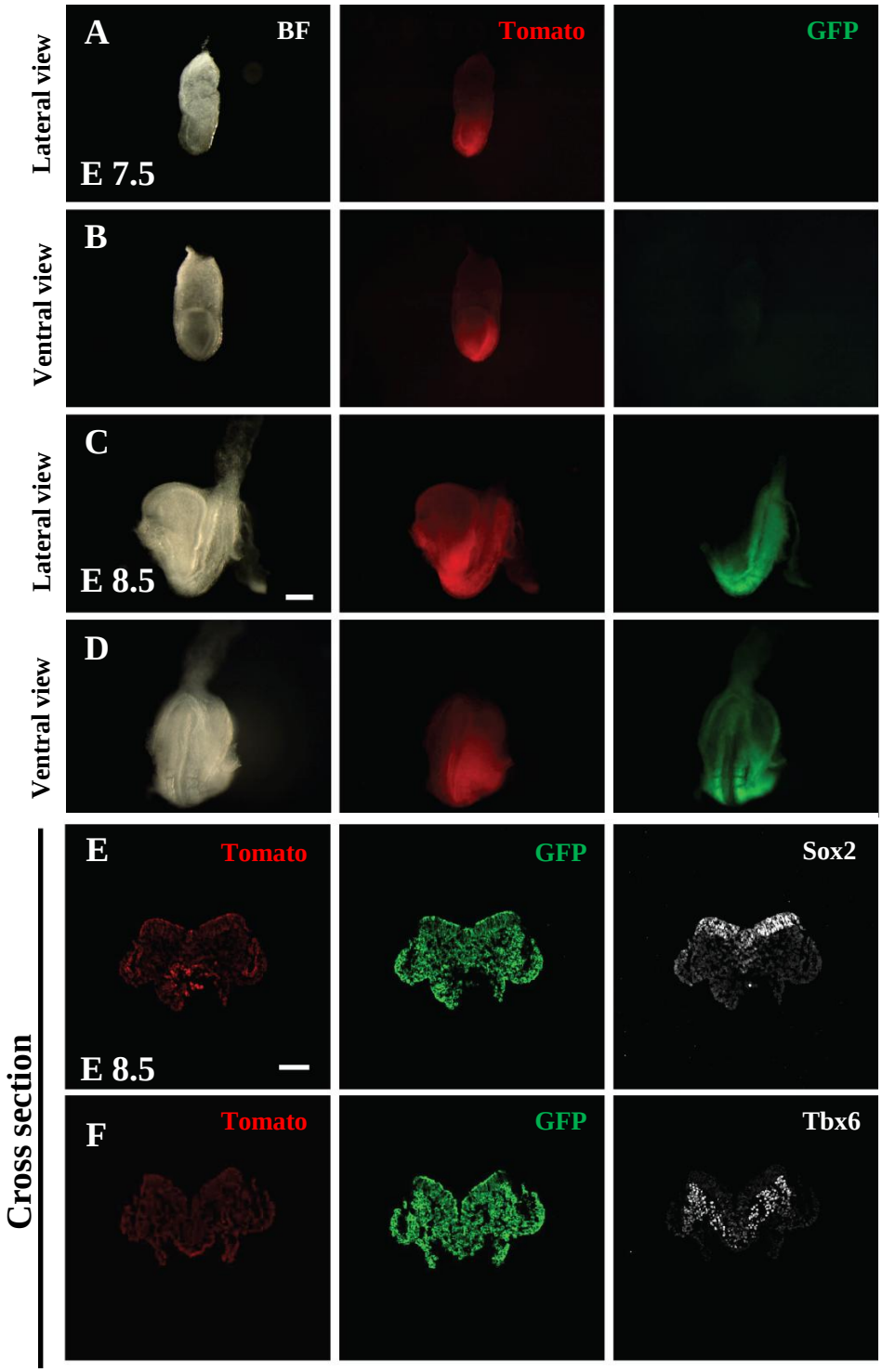


**Figure 22. Cre reporter *Rosa*$^{mTmG/mTmG}$ mated with *T-Cre***

Cre recombinase activity was investigated by crossing *Rosa*$^{mTmG/mTmG}$ with *T-Cre* mice. (A-D) Whole mount embryos images showing bright field (BF) and fluorescence of Tomato and GFP in the same embryo. Dot line in (C) showed the section plane of (E, F). Scale bar: 200μm. (E, F) Cross section analysis of *T-Cre*;*Rosa*$^{mTmG/mTmG}$ embryos of (C, D). Scale bar: 100μm. At E8.5, the Cre activity can be observed in PSM, lateral plate mesoderm and part of neural plate, overlapping with both Sox2 and Tbx6 expression domain (E, F).

# Figure 23

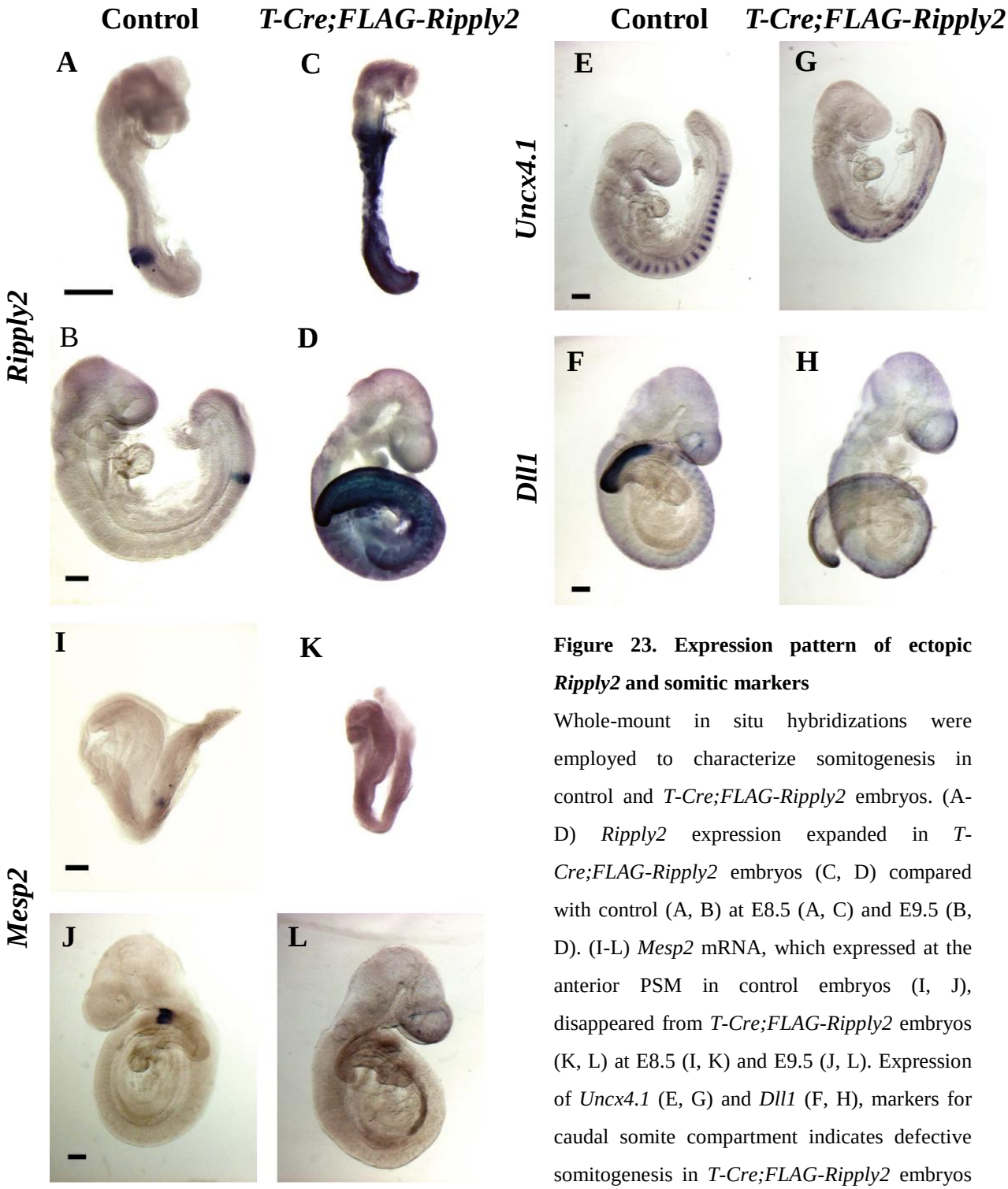


**Figure 23. Expression pattern of ectopic *Ripply2* and somitic markers**

Whole-mount in situ hybridizations were employed to characterize somitogenesis in control and *T-Cre;FLAG-Ripply2* embryos. (A-D) *Ripply2* expression expanded in *T-Cre;FLAG-Ripply2* embryos (C, D) compared with control (A, B) at E8.5 (A, C) and E9.5 (B, D). (I-L) *Mesp2* mRNA, which expressed at the anterior PSM in control embryos (I, J), disappeared from *T-Cre;FLAG-Ripply2* embryos (K, L) at E8.5 (I, K) and E9.5 (J, L). Expression of *Uncx4.1* (E, G) and *Dll1* (F, H), markers for caudal somite compartment indicates defective somitogenesis in *T-Cre;FLAG-Ripply2* embryos at E9.5. Scale bar: 200µm.

# Figure 24

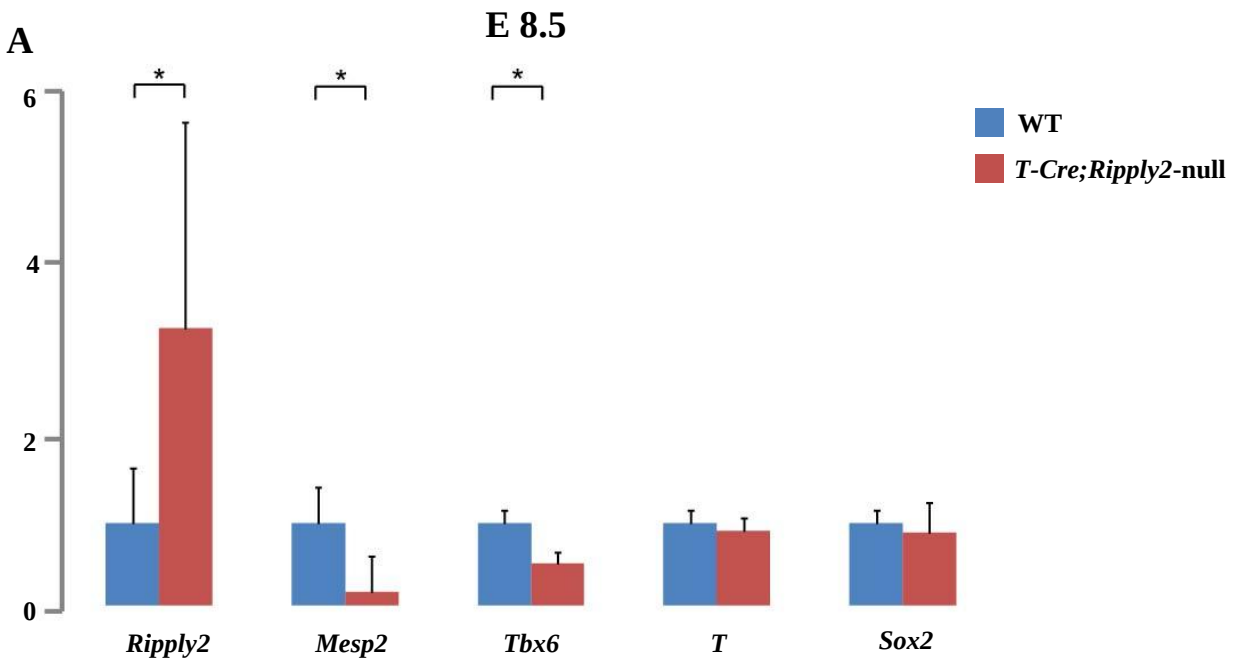


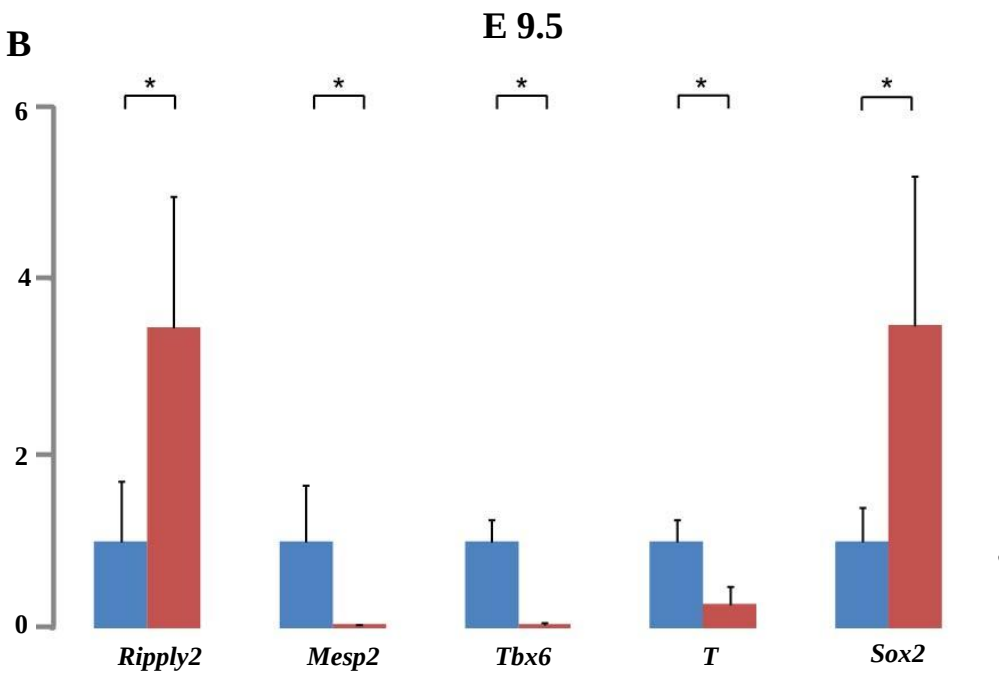


**Figure 24. Altered gene expression pattern in the ectopic Ripply2-expressing embryos**

RT-PCR analysis for the expression of *Ripply2*, *Mesp2*, *Tbx6*, *T*, and *Sox2* in unsegemented caudal region of control (n=6) and *T-Cre;FLAG-Ripply2* embryos (n=7) at E8.5(A) and control (n=4) *T-Cre;FLAG-Ripply2* embryos (n=4) at E9.5(B). $^{*}P < 0.05$ in Brunner-Munzel Test.

# Figure 25

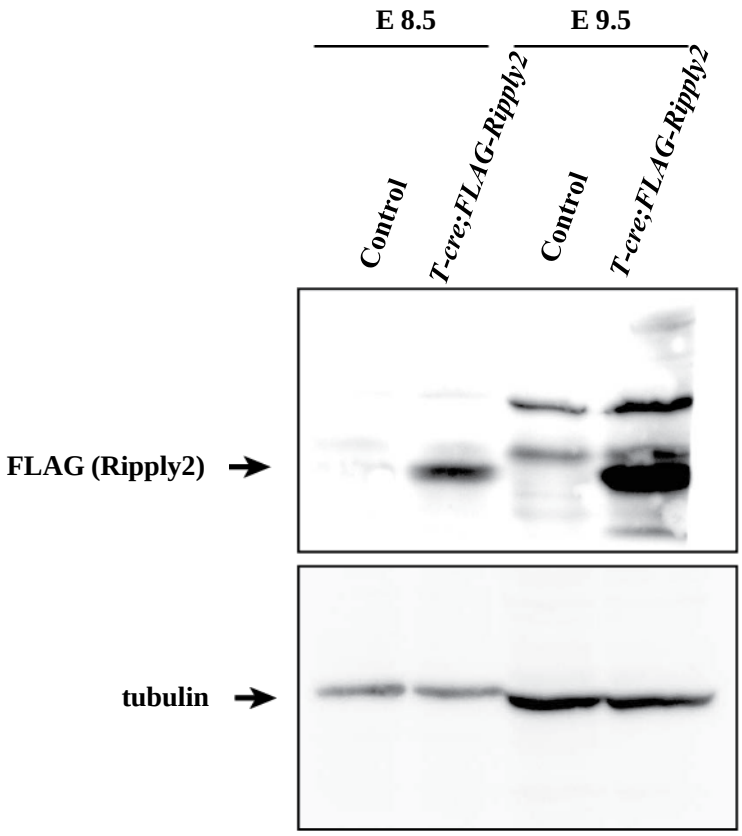


**Figure 25. Western blotting for ectopic Ripply2**

Anti-FLAG antibody recognized bind of FLAG-Ripply2 protein at E8.5 and E9.5 by western blotting in control and *T-Cre;FLAG-Ripply2* samples individually. Anti-β–tubulin antibody was used as a loading control.

# Figure 26

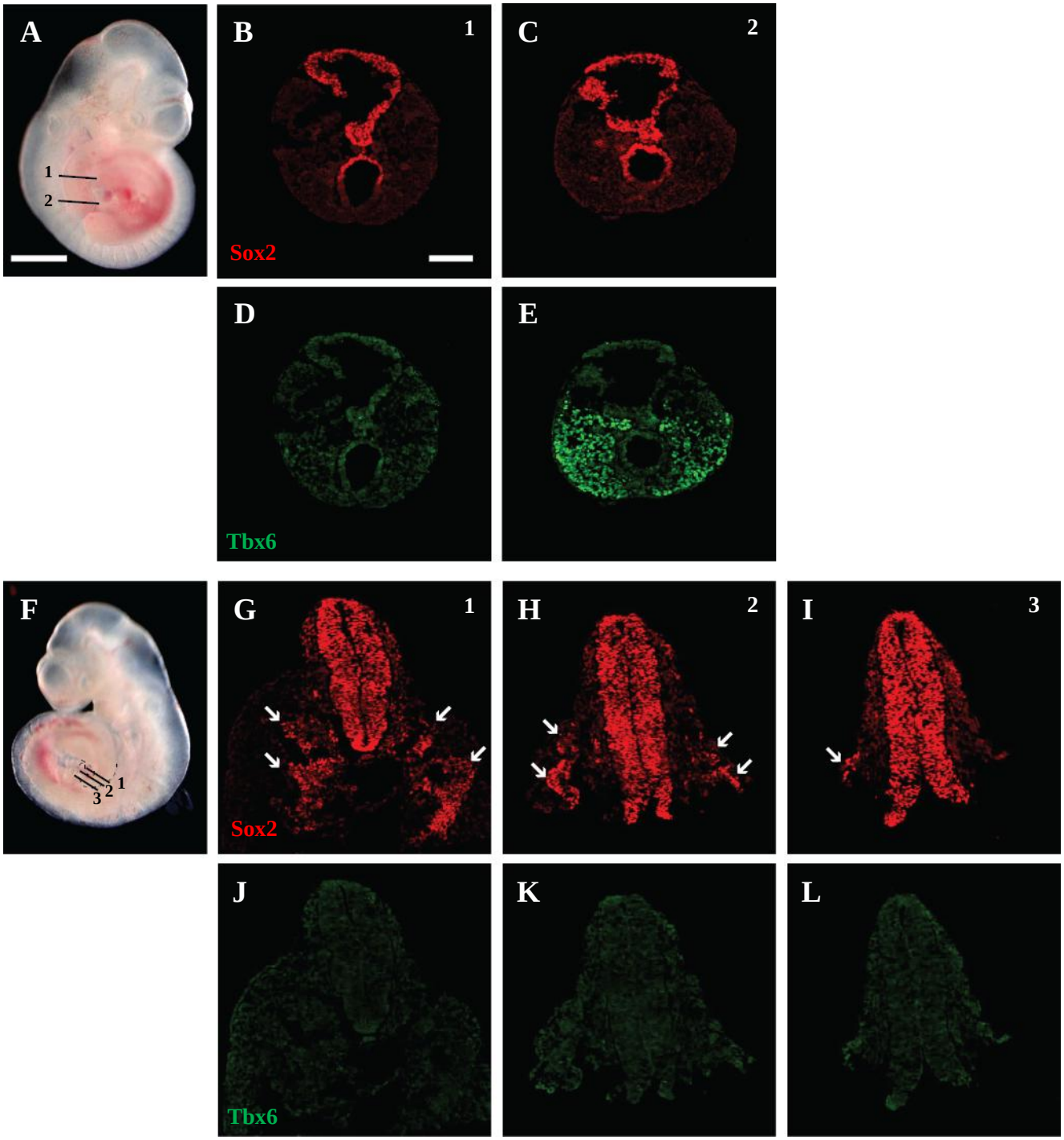


**Figure 26. Ectopic neural tube formation instead of the paraxial mesoderm in Ripply2-expressing embryos**

Cross sections were prepared from control at axial levels (1 and 2 in A) and from *T-Cre;FLAG-Ripply2* (1-3 in F) embryos at E10.5 and analyzed by immunostaining using anti-Sox2 (B-C, G-I) and anti-Tbx6 (D-E, J-L) antibodies. White arrows, ectopic neural tubes. Scale bar in A, 1mm for A and F. Scale bar in B, 100μm for others.

# Figure 27

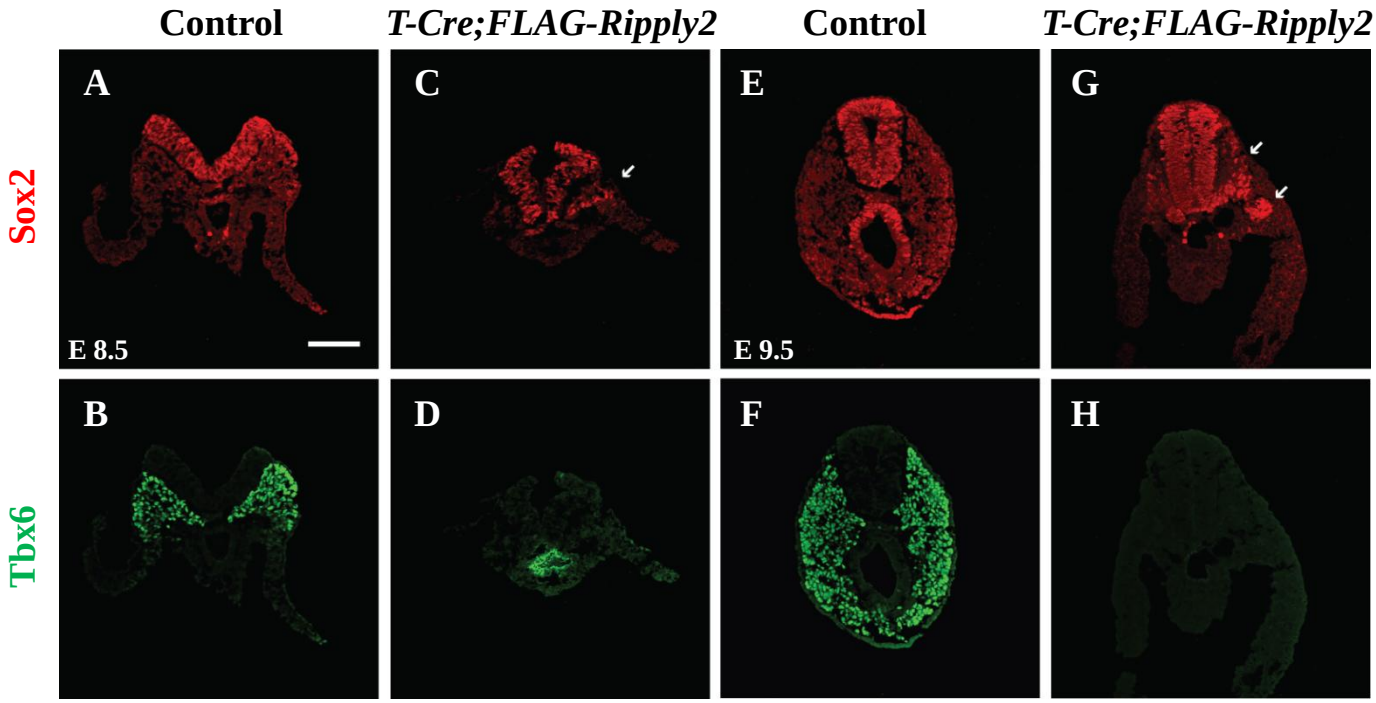


**Figure 27. Ectopically expressed Sox2 followed by neural tubes generated at bilateral region.**

Immunostaining for Sox2 (A, C, E, G) and Tbx6 (B, D, F, H) in cross sections of E8.5 (A-D) and E9.5 (E-H). In *T-Cre;FLAG-Ripply2* embryos, Tbx6 signal was almost undetectable (D) and the cells in the bilateral position underlying the neural plate expressed Sox2 at E8.5 (C). The ectopic Sox2 expression was followed by the ectopic development of neural tubes in the same compartment at E9.5 (G). White arrows, ectopic Sox2-positive cells. Scale bar: 100μm.

# Figure 28

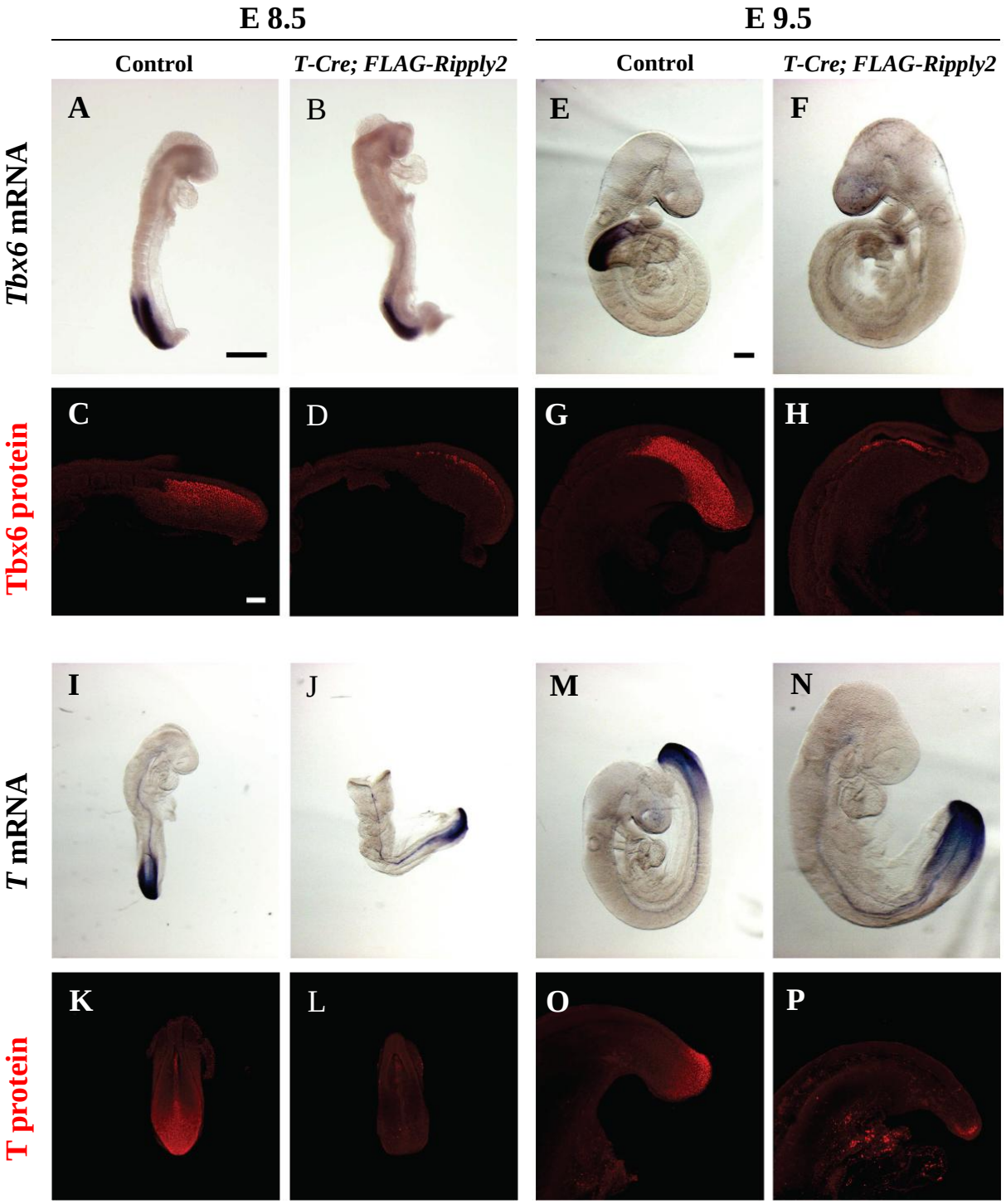


**Figure 28. Protein expression rather than mRNA of T and Tbx6 are influenced by ectopic Ripply2**

Expression changes induced by ectopic Ripply2 were examined at the levels of mRNA and proteins for Tbx6 and T at E8.5 (A-D, I-L) and E9.5 (E-H, M-P). (A-H) *Tbx6* mRNA (A, B, E, F) and Tbx6 protein (C, D, G, H) in control (A, C, E, G) and *T-Cre;FLAG-Ripply2* embryos (B, D, F, H). (I-P) *T* mRNA (I, J, M, N) and T protein (K, L, O, P) in control (I, K, M, O) and *T-Cre;FLAG-Ripply2* embryos (J, M, N, P). Scale bar: 200µm for (A, B, E, F, I, J, M, N). Scale bar: 100µm for (C, D, G, H, K, L, O, P).

# Figure 29

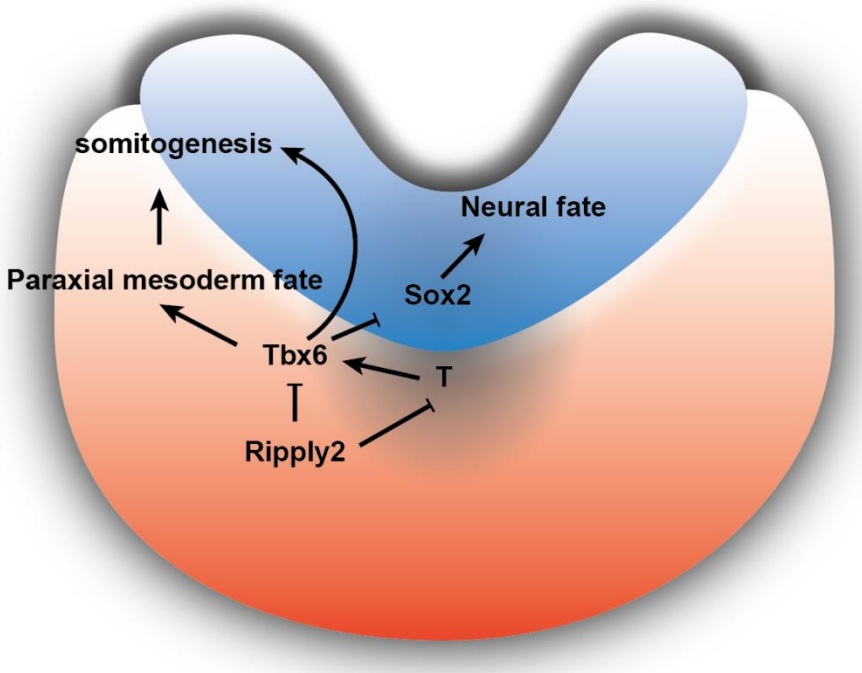


**Figure 29. Model of the regulatory signaling network during generation of neural tubes and paraxial mesoderm**

# Figure 30

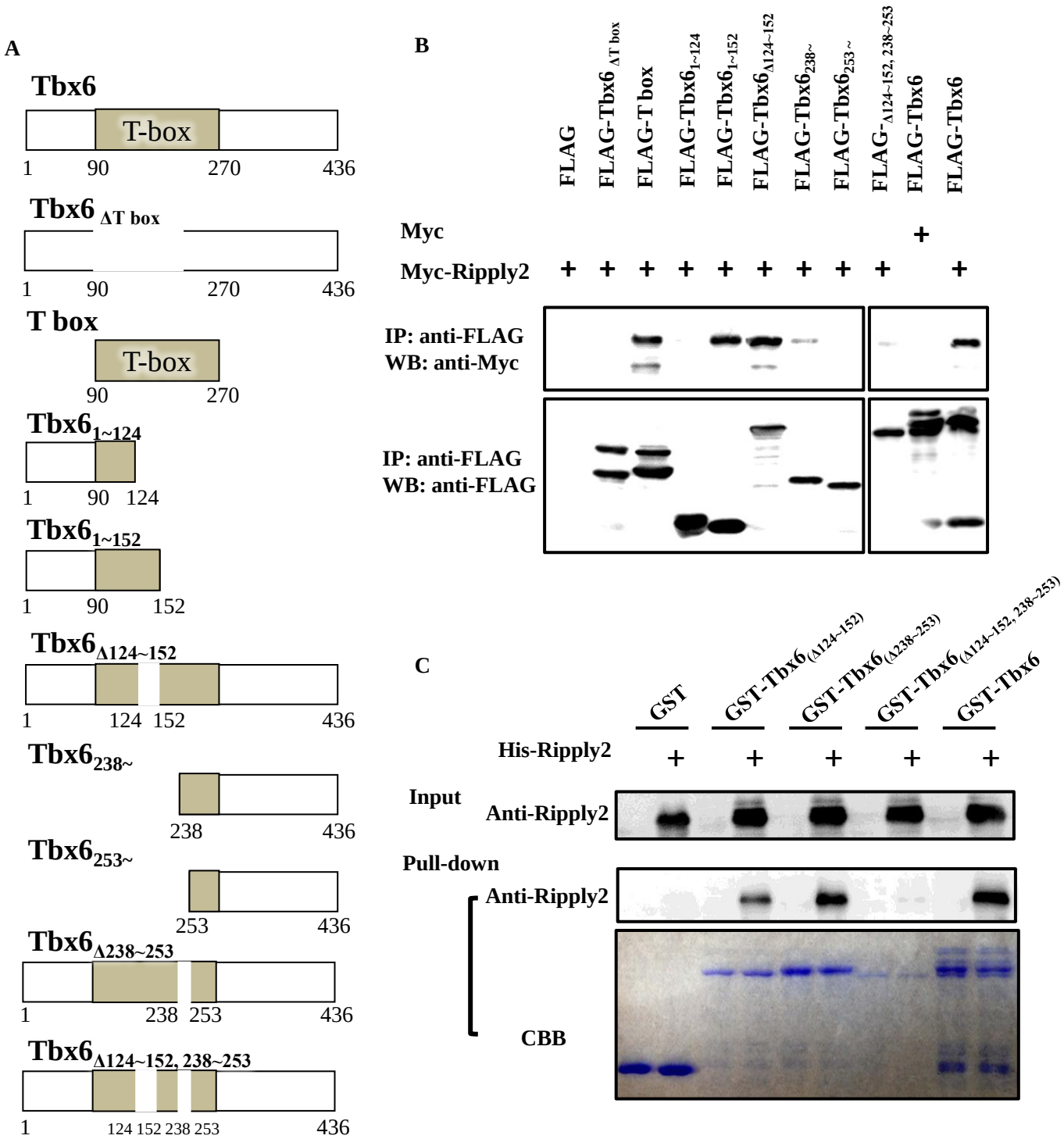


**Figure 30. Tbx6 has two Ripply2-binding domains.**

(A) Schematic diagram of Tbx6 and its deletion mutants. (B) Identification of Ripply2 binding sites on Tbx6. T-box domain alone was sufficient to immunoprecipitate Myc-Ripply2. The residues 124~152 and 238~253 in Tbx6 contribute to its interaction with Ripply2. (C) GST pull-down assay was performed to examine the direct binding between Tbx6 and Ripply2. $Tbx6_{(\Delta 124\sim152)}$ and $Tbx6_{(\Delta 238\sim253)}$ but not $Tbx6_{(\Delta 124\sim152,\ 238\sim253)}$ interacte with Ripply2.

# Figure 31

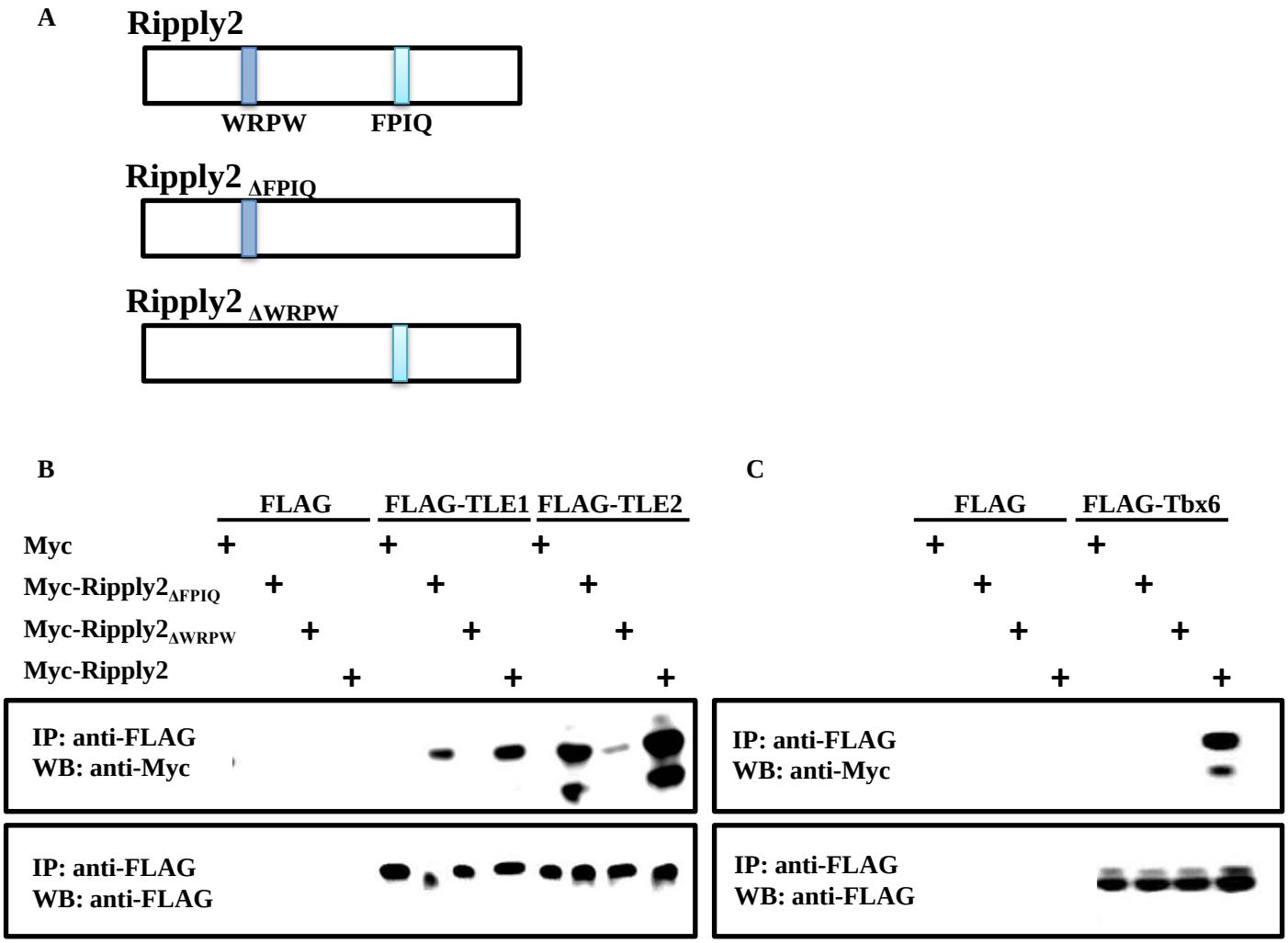


**Figure 31. Ripply2 interacts with Tbx6 via Ripply homology domain (FPIQ) and with Groucho/TLE via WRPW domain.** (A) Schematic diagram of Ripply2 and its deletion mutants. (B) Interaction between mouse Ripply2 and TLE1/2. Four amino acid residues FPIQ is necessary for this binding. (C) The deletion of either FPIQ or WRPW result in lost of binding Tbx6.